Title: Future malaria environmental suitability in Africa is sensitive to hydrology

Authors: Mark W. Smith[1]*, Thomas Willis[1], Elizabeth Mroz[1], William H. M. James[1], Megan J. Klaar[1], Simon N. Gosling[2], Christopher J. Thomas[3,4]

Affiliations:

[1]School of Geography and Water@Leeds, University of Leeds; Leeds, LS2 9JT, United Kingdom.

[2]School of Geography, University of Nottingham; Nottingham, NG7 2RD, United Kingdom.

[3]School of Geography and Lincoln Centre for Water and Planetary Health, University of Lincoln; Lincoln, United Kingdom.

[4]University of Namibia; Windhoek, Namibia

*Corresponding author. Email: m.w.smith@leeds.ac.uk

Abstract: Changes in climate shift the geographic locations that are suitable for malaria transmission owing to thermal constraints on vector *Anopheles* mosquitos and *Plasmodium* spp. malaria parasites and the availability of surface water for vector breeding. Previous Africa-wide assessments have tended to solely represent surface water using precipitation, ignoring many important hydrological processes. Here, we apply a validated and weighted ensemble of global hydrological and climate models to estimate present and future areas of hydro-climatic suitability for malaria transmission. With explicit surface water representation, we predict a net decrease in

areas suitable for malaria transmission from 2025 onwards, greater sensitivity to future greenhouse gas emissions and different, more complex malaria transmission patterns. Notably, areas of malaria transmission that are projected to change are smaller than estimated by precipitation-based estimates, but associate with greater change in transmission season lengths.

5

One-Sentence Summary: Hydrological models project that areas of malaria risk will decrease as climate change proceeds with more focused and intense transmission changes.

Main Text:

Malaria is a climate-sensitive vector-borne disease that caused 619,000 deaths among 247 million cases in 2021 (*1*). This burden is acutely focused on Africa, where 95% of global cases are reported (*1*). Reductions in cases in Africa have slowed or even reversed in recent years, attributed in part to a stall in investments in global responses to malaria control. To build resilient health systems we must understand present-day malaria transmission and potential future areas of malaria risk (*2*). Malaria transmission is a function of many complex and interacting parameters (*3*), including strong environmental controls. Given these interactions and in the face of rapidly changing climate in Africa, it is important not only to model the impact of these controls on changing malaria transmission hazard *per se*, but also to improve the climate-process representation. Doing so will facilitate future integration with estimated changes in other key sectors (e.g., agriculture), to identify intersecting impacts and potential trade-offs (*4-6*).

Ambient air temperature influences sporogonic and gonotrophic development rates, biting rates and vector longevity (*7*). Persistent surface water is required for vector breeding sites that remains at an appropriate temperature for larval development (*8-10*). Thermal response models for malaria are relatively well understood (*11*) and readily implemented within studies examining future climate-driven shifts in disease transmission suitability (*12*). By contrast, the controls on surface water availability for vector breeding are either ignored or poorly represented within climate-driven geospatial models of transmission suitability.

Assessments at regional or village scales typically represent detailed hydrological processes (*8*, *13*) and they are increasingly incorporated into malaria transmission models (*14*, *15*). However, continental and global scale analyses lack detailed parameterisation of hydrological processes and conventionally apply a rainfall threshold as a proxy for water body

availability (typically 60–80 mm month^{-1}, although a wide range is observed) (*9*, *16-19*). Such a simple threshold bypasses many important hydrological processes. Rainfall is not a good indicator of standing water availability (*12*) and the resulting estimates for malaria occurrence are sensitive to the specific choice of precipitation threshold (*20*). Initial findings suggest that process-based representations of breeding habitat availability results in a more complex pattern of areas estimated to be suitable for malaria transmission across Africa, as infiltration, evaporation, runoff and river discharge are directly represented (*20*).

Here, we address the challenge of incorporating robust estimates of vector breeding site availability into continental-scale estimates of areas of suitability for malaria transmission. The application of a single hydrological model presented in our earlier work *(20)* is problematic, as diverse different hydrological models are available (*21*), each reflecting the perceptual models and focuses of their creators (*22*), which means the outputs (e.g., surface water) of one model can be quite different from another (*23*) and performance (i.e., simulation compared to observation) can vary considerably (*24*). Recognising these limitations, we present a multi-model multi-scenario ensemble of global hydrological and global climate models (*25*), weighted based on model performance, to estimate present and future distribution of malaria suitable areas across Africa. We examine the sensitivity of malaria distribution estimates to different hydrological models and evaluate multiple hydrologically informed metrics to represent breeding site availability. Critically, inclusion of hydrological modelling identifies future shifts in the distribution of malaria suitable areas to a precipitation-based estimate. Finally, we quantify the human populations impacted by changing lengths of malaria transmission season as future climate changes alter hydro-climatic suitability for malaria transmission.

Variability in malaria suitability estimates

We calculated the distribution of malaria suitable areas for 1986-2005 using hydrological outputs from seven Global Hydrological Models (GHMs), which were each driven with climate data from four Global Climate Models (GCMs). When a precipitation threshold is used to represent surface water availability, estimates of areas suitable for malaria transmission across the GCMs show very limited variability (Fig. 1B, Fig. S1), as shown by the strong agreement among estimates. In contrast, explicit representation of hydrological processes using the GHMs shows greater variability in projections for areas of malaria transmission, reflecting different structures among hydrological models. Although total extents of hydro-climatic suitability (i.e., the length of transmission season (LTS) > 1 month) were similar across the GHMs (Fig. S2), estimates from the ORCHIDEE model show particularly large areas of endemic malaria (> 9 months continuous transmission suitability) while the LPJml showed the least extent of endemic malaria.

Continental-scale malaria distribution patterns are broadly similar for each hydrological representation we examined, although hydrology-based estimates are patchier than precipitation-based estimates. However, hydrological estimates are more physically realistic and identify larger areas with year-round malaria (Fig. 1). Large-scale river networks are highlighted as local foci of endemic malaria, particularly the Nile. With human population centres typically located around large waterways, these differences are more significant when considering the number of people residing in potentially malaria endemic areas (29 million people at risk using precipitation-based estimates compared with 107 million people at risk when discharge is used). While malaria transmission may not be observed in all these locations today thanks to successful interventions, they nevertheless remain hydro-climatically suitable for transmission.

To represent the likelihood of temporary rain-fed puddles forming, while also incorporating water fluxes within continental-scale river networks, the potential evapotranspiration to precipitation ratio was calculated and hydrological suitability computed. This ratio provides a basic surface water balance and was added to the discharge suitability layer (Q_PE). Including the local surface runoff expands the area further with larger areas suitable for >3 months per year. Conversely, the additional criteria of a minimum relative humidity threshold restricts this suitable area, notably at the northern extent, particularly Chad, Mali and Sudan. However, active transmission in eastern Sudan has been observed in proximity to rivers even in hot dry seasons (*26*).

Calculation of variance ratios shows that GHMs are the primary influence, with GCMs contributing only 2% of variance in endemic malaria areas, 7% for areas of seasonal malaria and 16% for all areas >1 month suitability for the Q_PE hydrological representation. For discharge alone, the values are lower (all 2% or less) but when including the additional relative humidity threshold, the values are slightly higher, owing to the additional climate dependency (Fig. 1G). When examining sources of variance in LTS estimates for each grid cell, Fig. 1G highlights the overall dominance of GHMs, although GCMs are locally important in the Ethiopian highlands and other high-altitude areas of East Africa, in areas at the northern fringe of transmission suitability and an isolated area in Mozambique.

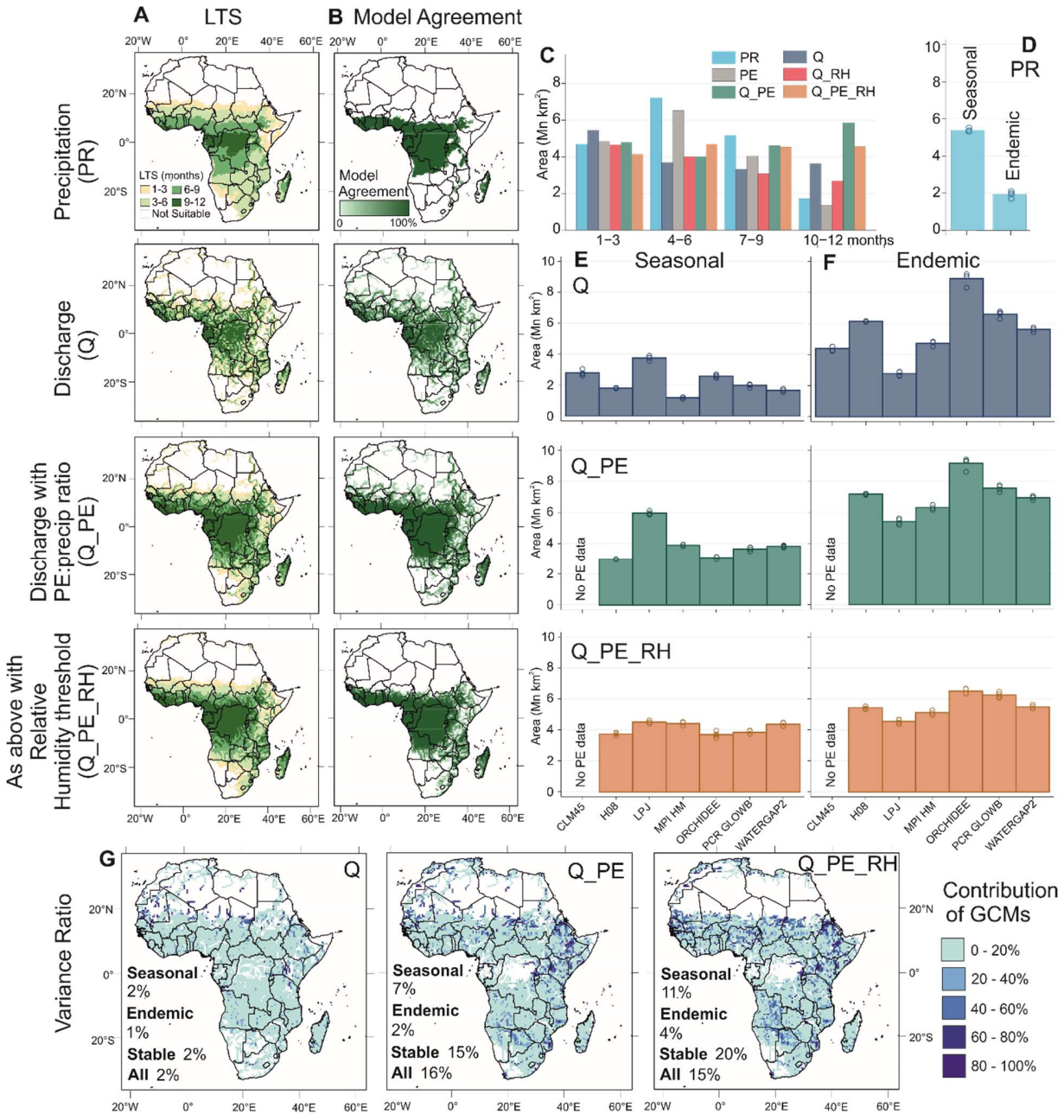

Fig. 1. Variability in malaria hydro-climatic suitability estimates (1986-2005). (**A**) Mean Length of Transmission Season (LTS, in months) estimates for each hydrological representation (mean of all GCM and GHM combinations). (**B**) Model agreement across each ensemble. Maps indicate the percentage of models in the ensemble that estimate LTS > 6 months (full data

presented in Fig. S1 and Table S1). (**C**) LTS estimates for each hydrological representation calculated within 3-month bands using the model ensemble weightings established in later validation. (**D**-**F**) Estimates of seasonal (LTS > 6 months) and endemic malaria suitability (LTS > 9 months) showing all individual model estimates across different hydrological models (bars showing mean value) and global climate models (individual points for each climate model, n = 4). Precipitation is plotted separately in (D). (**G**) Variance ratios for all hydrology-derived layers showing the percentage of variance in malaria LTS contributed by GCMs for each model cell.

Ensemble weighting and model performance

Validation of estimates of hydro-climatic suitability is problematic because malaria transmission is driven by non-climatic factors, notably successful interventions reducing the geographic spread of transmission (*3*). We also recognise that sub-Saharan vector species vary in their larval habitat requirements (*27*), and often use small, shallow sunlit water-filled depressions such as hoof prints, wheel ruts and puddles for breeding sites (e.g., *An. gambiae sensu stricto* and *An. arabiensis*), though even here habitat hydrology and geomorphology have been shown to control the distribution of malaria vector larva (*28*). Conversely, other major vectors (e.g., *An. funestus*) require semi-permanent fresh water bodies such as swamps, ponds and lake edges (*27*) and secondary vectors such as *An. Coustani* and *An. Squamosus* breeding in large, vegetated floodplains connected to rivers can be locally and regionally important vectors (*29,30*). Local variability in vector ecology presents a challenge to any geographically uniform approach to model malaria suitability (*31*), though the inclusion of both local runoff and large-scale water fluxes in the composite hydrological metric (Q_PE) is an attempt to ensure both habitat types are represented.

We validate malaria suitability estimates for the preindustrial period 1875-1900 against the pre-intervention map of Lysenko and Semashko (*32*) (Fig. 2A) which approximates malaria extents at ~1900 AD. The performance of each model is used to allocate a model weight in an ensemble for future predictions of extent (see Materials and Methods, Figs. S3-S5 and Tables S2-S5 for details).

Ensemble estimates are shown in Fig. 2B and Figs. S6 and S7 with estimates compared against observations in Fig. 2F and Fig. S8. Hydrology-based estimates (discharge with potential evapotranspiration) performed only very slightly better than estimates made with precipitation alone (ensemble score of 0.817 vs 0.816) and a relative humidity filter reduced this performance owing to underestimation in the northern fringes of transmission. All models are slightly biased towards under-prediction (negative bias scores in Fig. 2C). The spatial extent of pre-industrial malaria suitability estimates is broadly similar to those of the historical period presented in Fig. 1, with the more substantial increases in suitability observed at high elevations in East Africa focused on Ethiopia and Uganda (Fig. S3).

Overall, validation shows a close match between modelled and observed suitability. All models overestimate the extent of areas suitable for mosquito breeding in South Africa, but the northern fringes of the transmission zone are correctly represented, with only minor underestimates (Fig. 2F). Similarly, areas suitable for malaria transmission in the Horn of Africa are underestimated in all models. All models underestimate the potential for malaria transmission along the North African coast, although here hydrology-based estimates outperform the precipitation-based estimates. The presence of different malaria vector species in North Africa with different thermal ranges to the typical sub-Saharan species (*33*) may explain this

discrepancy. Some over-estimation is evident in the Sahara for the hydrological model output (without the relative humidity filter), where the course of the now dry Tamanrasset palaeoriver (*34*) is identified as suitable for malaria transmission for individual months. However, the Nile corridor of malaria risk in Egypt, where malaria was endemic until the 1990s, is only identifiable in the models that describe discharge and discharge with potential evapotranspiration (*35*). The relative humidity threshold applied at this grid scale appears to be overly restrictive and cannot represent the fine-scale local influence of water bodies on air humidity. Overall, there is no strong evidence to distinguish between the performance of precipitation and discharge with potential evapotranspiration representations (Fig. 2D). Further validation of weighted layers for the 1986-2005 time period against anopheline observations (*36*), parasite ratios (*37*) and modelled probabilities of occurrence of *Anopheles gambiae* (*38*) (Fig. S9, Table S6) confirm that both precipitation and discharge with potential evapotranspiration representations perform equally well. Thus, future suitability estimates from both are considered in Fig. 3.

Future projections of declining malaria risk

For the RCPs 2.6 and 6.0 model ensembles there is agreement that a modest initial increase in areas of hydro-climatic suitability for malaria transmission (2006-2025; <0.5 Mn km^2) is followed by an overall decline (Tables S7-S8) to 2100. RCP2.6 predicts the greatest increase in malaria transmission suitability, which reverses by 2075-2100. Conversely, RCP 8.5 shows little or no initial increase prior to a more substantial decline in area. Considering only areas where the signal-to-noise ratio >0.5, both hydrological and precipitation-based estimates agree that the overall hydro-climatic suitability for malaria transmission decreases from the baseline period (Fig. 3). The decreasing area suitable for malaria transmission becomes more pronounced

through time and for higher greenhouse gas emissions scenarios (RCP 6.0 and RCP 8.5), although it should be noted that hydrological estimates show greater sensitivity to the choice of RCP than precipitation-based malaria suitability estimates (Fig.3B vs 3F).

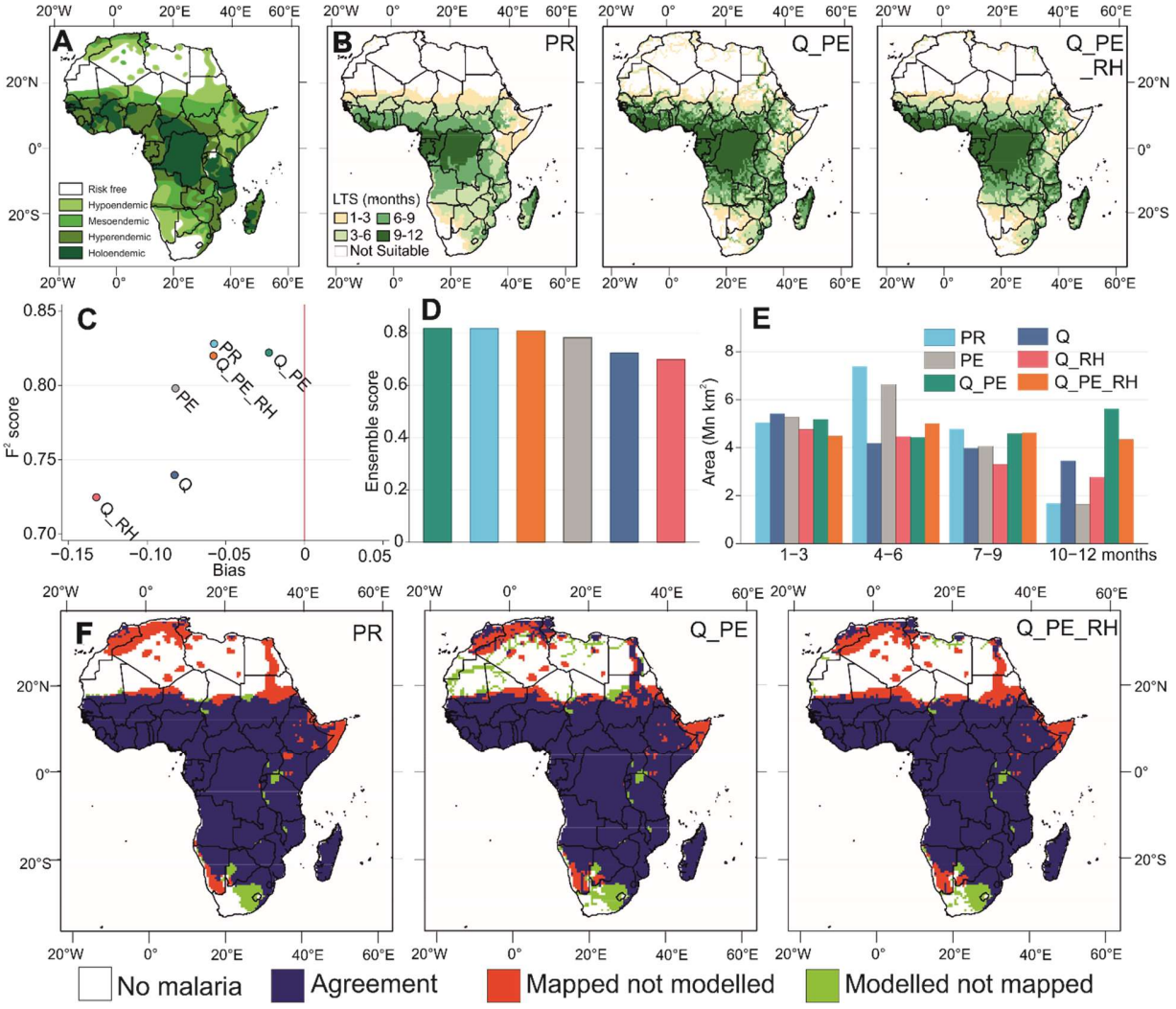

Fig. 2. Validation of model hydroclimatic malaria suitability estimates. (**A**) Pre-intervention malaria map of Lysenko and Semashko (*32*); (**B**) weighted ensemble model estimates of hydro-climatic malaria suitability LTS (1875-1900); (**C-D**) summary of ensemble validation metrics for each hydrological representation, with both metrics plotted separately and combined as an

ensemble score (full data in Tables S2-S3); (**E**) estimates of malaria suitability by the weighted ensembles for each hydrological representation calculated within 3-month bands; (**F**) selected validation maps comparing observed and modelled malaria suitability (where at least one month is suitable). Figs. S6-S9 present validation maps and LTS maps for all hydrological representations.

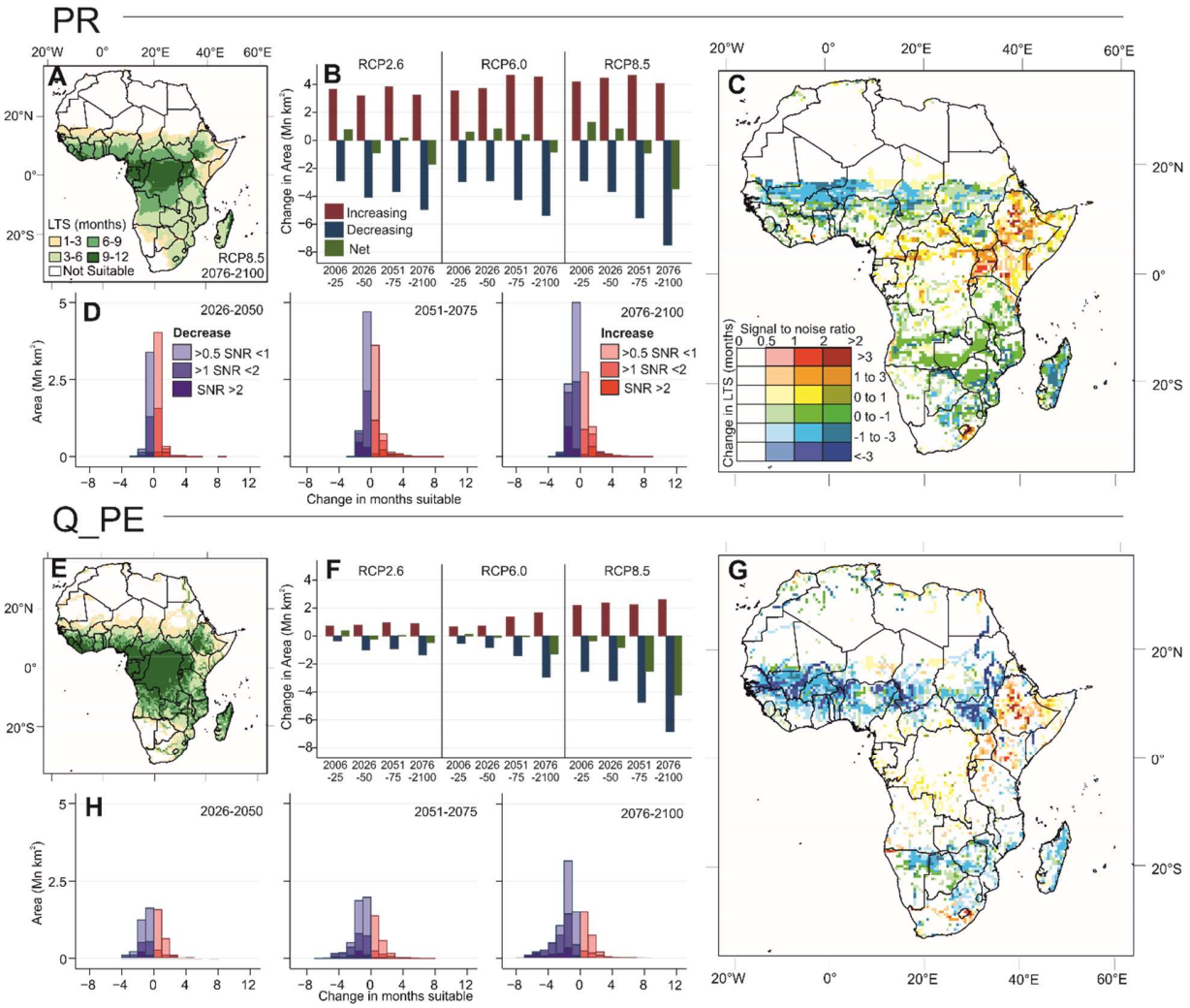

Fig. 3. Future projections of malaria hydro-climatic suitability. (**A**, **E**) Projected Length of Transmission Season in RCP 8.5 for 2076-2100. Areas showing an increase or decrease in

suitability since 1986-2005 across all scenarios and time periods are plotted in (**B**, **F**) showing only areas with a signal-to-noise ratio (SNR) > 0.5. The locations of these changing areas are shown for RCP 8.5 (2076-2100) in (**C**, **G**) and for all RCP scenarios and time periods in Fig. S11. The extent of change in suitability (number of months change) is plotted by signal-to-noise ratio as stacked histograms for RCP 8.5 in (**D**, **H**) and for all scenarios in Fig. S12.

Precipitation-based estimates show a larger shift in the geographical locations of malaria transmission suitability, with large areas (3-4 Mn km^2) experiencing increasing malaria risk in all RCPs and time periods (mostly greater than twice that of the hydrology-based estimates; Table S9) that are offset by growing areas of decreasing suitability for malaria transmission (> 2 million km^2). By contrast, hydrology-based estimates show smaller areas increasing in suitability for malaria, and a greater sensitivity to the RCP, particularly for the areas diminishing in malaria suitability (Fig. 3). Precipitation-based estimated changes are mostly small (a reduction in the LTS by 1 month, Fig. 3D); conversely, hydrology-based estimates show substantial areas where suitability for malaria transmission decreases by 4 months or more (Fig. 3H; Fig. S12). Thus, projected changes using hydrology-based estimates are more concentrated but also more intense when compared with precipitation-based estimates. Calculation of the overall magnitude of the change (i.e., the product of the change in LTS in months and the area) shows the reduction in suitability is more pronounced in the hydrology-based estimates, but only for RCP 8.5, where it is more than double precipitation-based estimates by 2076-2100 (Fig. S10 and Table S10).

The pattern of projected changes in malaria distribution is markedly different between precipitation and hydrology-based estimates (Fig. 3C and G; Fig. S11). While both approaches

identify future declines in malaria transmission across West Africa, the area experiencing a reduction in LTS is more extensive with hydrology-based estimates, stretching as far east as South Sudan. Increases in areas of malaria risk in the highlands of Ethiopia are expected to expand (although to a lesser extent than modelled previously (*39*)), but the increase in projected malaria prevalences for Kenya, Uganda and the north of the Democratic Republic of the Congo estimated by precipitation-based models are not seen for any RCP. Small decreases in the LTS of <1 month across Tanzania and Zambia are also not observed with any hydrology-based estimates, but for RCP 8.5 a stronger focus of decreasing risk emerges further south in Mozambique, Zimbabwe, Botswana and Namibia. Finally, the small area of increasing malaria risk centred on Lesotho is seen in all estimates, but also stretches west along waterways (specifically the Orange River where flood-driven malaria has been observed historically (*40*)) when fluvial water transfer is represented in the hydrology-based estimates.

At the country level, inclusion of hydrological processes in malaria distribution models results in larger modelled decreases in LTS, when compared with precipitation based estimates, in those countries where the projected changes are focused (particularly West Africa and the northern fringes of malaria transmission suitability; Fig. S13). Future estimated populations at risk show considerable growth in areas having longer estimated periods of malaria transmission suitability (Fig. 4). The difference between precipitation and hydrology-based estimates is particularly pronounced for endemic areas with LTS >9 months, with the populations affected being four-times greater when hydrology is represented. Again, this highlights the combination of waterways as centres for human population growth and foci for malaria risk (Figs S14-S16 and Table S11).

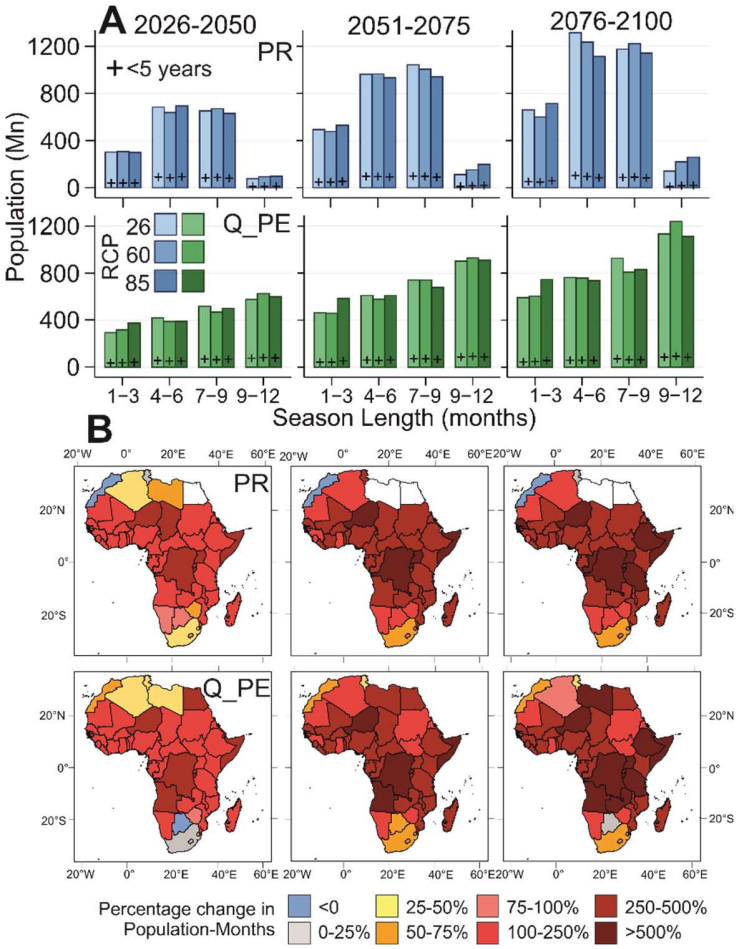

Fig. 4. Future populations in areas hydro-climatically suitable for malaria transmission. (**A**) Populations within 3-month bands of LTS for both precipitation and discharge with potential evapotranspiration hydrological representations. Bars show total populations for each RCP for each weighted ensemble. Points indicate population under-5 years old. Populations calculated using UN medium variant projections for each period. (**B**) Predicted percentage changes in population-months (i.e., population exposed multiplied by the number of additional months of exposure) since 1986-2005 by country for RCP 8.5 only (see Fig. S13 for each RCP). White indicates no estimated malaria suitability.

Discussion

Changes in malaria transmission are complex and not driven by climate alone; yet, the effect of climate change on malaria prevalence is pronounced, particularly in Africa (*2*). Many models have been used to estimate future transmission risk using simple precipitation-based approaches; however, positive correlations between malaria and rainfall are not consistent (*41*). We present a multi-model ensemble of hydrological and global climate models to estimate changes in malaria transmission risk, which reveals substantial variability in estimates from different hydrological models and the value of an ensemble approach where models are evaluated based on historical performance (*42*, *43*). GHM ensembles are now routinely used within climate change impact assessments (e.g., *5*, *23*, *44-46*); however, these have not previously been applied to represent malaria transmission.

As river systems are directly represented in a hydrological approach, the largest differences between precipitation-based and hydrology-based malaria estimates are observed near rivers and floodplains, which are also the largest population foci. As a consequence, hydrology-based approaches indicate that the number of people residing in potentially malaria endemic areas is four-times that estimated with precipitation-based estimates. There is also a greater sensitivity of malaria outcomes to the choice of RCP when hydrology is simulated explicitly. There is general agreement that malaria transmission will decrease across much of West Africa, as also predicted in previous studies (e.g., *13*, *18*, *20*, *47*), although when the hydrological processes that determine viable vector habitat formation are modelled explicitly, estimates for transmission

decrease more extensively. The warming and drying trends underlying this decrease in areas suitable for malaria themselves present profound environmental and social challenges (*48*), not least other predictions that this trend will increase dengue suitability (*49*).

Embedding GHM estimates of hydrological suitability for vector breeding directly into process-based malaria models such as VECTRI and LMM (*14*, *15*) will permit a more direct evaluation of transmission intensity in future. Differences in mosquito ecology and breeding habitat preferences across Africa are not presently included in the model. Representing the regional variability in mosquito vectors while also partitioning modelled surface water bodies by mosquito species breeding site preferences would more directly represent this important source of variability. However, this information is currently beyond the capabilities of GHM ensembles and would require a more hydrodynamic approach. While more detailed hydrological treatments have already been tested at regional or village scales (*8*), currently, the spatial resolution of available data limits our ability to model individual water bodies explicitly at the continental scale or to identify specific *Anopheles* vector niches.

The continental-scale evaluation of malaria climate change impacts using GHM ensembles presented here imposes the relatively coarse half-degree grids that are presently the main limitation of this approach. Finer details of waterbody dynamics such as the flushing of habitat require higher resolution models of individual floodplains. Situations where drought and falling river levels causes flow disconnection and formation of isolated stream-bed water bodies that function as suitable breeding habitats (*9*) are not well captured by our current approach. As these data sources become increasingly available, we will benefit from their explicit incorporation in

projections of hydrological processes to explain physically realistic malaria transmission risk at scales that can inform national operational malaria control strategies.

References and Notes

1. World Health Organisation, “World Malaria Report 2022” (World Health Organization, Geneva, 2022); https://www.who.int/teams/global-malaria-programme/reports/world-malaria-report-2022

2. M.A. Kulkarni, C. Duguay, K. Ost, Charting the evidence for climate change impacts on the global spread of malaria and dengue and adaptive responses: a scoping review of reviews. *Globalization and Health* **18**, 1-18. (2022).

3. P.W. Gething, D.L. Smith, A.P. Patel, A.J. Tatem, R.W. Snow, S.I. Hay, Climate change and the global malaria recession. *Nature* **465**, 342–345 (2010).

4. L. De Vos, H. Biemans, J.C. Doelman, E. Stehfest, D.P. van Vuuren, Trade-offs between water needs for food, utilities, and the environment—a nexus quantification at different scales. *Environmental Research Letters* **16**, 115003 (2021).

5. W. Thiery, S. Lange, J. Rogelj, C.F. Schleussner, L. Gudmundsson, S.I. Seneviratne, M. Andrijevic, K. Frieler, K. Emanuel, T. Geiger, D.N. Bresch, Intergenerational inequities in exposure to climate extremes. *Science* **374**, 158-160 (2021).

6. M. Giuliani, J.R. Lamontagne, M.I. Hejazi, P.M. Reed, A. Castelletti, Unintended consequences of climate change mitigation for African river basins. *Nature Climate Change* **12**, 187–192 (2022).

7. L.L. Shapiro, S.A. Whitehead, M.B. Thomas, Quantifying the effects of temperature on mosquito and parasite traits that determine the transmission potential of human malaria. *PLoS Biology* **15**, 2003489 (2017).

8. A. Bomblies, J.B. Duchemin, E.A. Eltahir, Hydrology of malaria: Model development and application to a Sahelian village. *Water Resources Research* **44**, W12445 (2008).

9. M.W. Smith, M.G. Macklin, C.J. Thomas, Hydrological and geomorphological controls of malaria transmission. *Earth-Science Reviews* **116**, 109-127 (2013).

10. M.N. Bayoh, S.W. Lindsay, Effect of temperature on the development of the aquatic stages of *Anopheles gambiae* sensu stricto (Diptera: Culicidae). *Bulletin of Entomological Research* **93**, 375–381 (2003).

11. E.A. Mordecai, K.P. Paaijmans, L.R. Johnson, C. Balzer, T. Ben-Horin, E. de Moor, A. McNally, S. Pawar, S.J. Ryan, T.C. Smith, K.D. Lafferty, Optimal temperature for malaria transmission is dramatically lower than previously predicted. *Ecology Letters* **16**, 22-30 (2012).

12. S.J. Ryan, C.A. Lippi, F. Zermoglio, Shifting transmission risk for malaria in Africa with climate change: a framework for planning and intervention. *Malaria Journal* **19**, 1-14 (2020).

13. T.K. Yamana, A. Bomblies, E.A. Eltahir, Climate change unlikely to increase malaria burden in West Africa. *Nature Climate Change* **6**, 1009-1013 (2016).

14. V. Ermert, A.H. Fink, A.E. Jones, A.P. Morse, Development of a new version of the Liverpool Malaria Model. I. Refining the parameter settings and mathematical formulation of basic processes based on a literature review. *Malaria Journal* **10**, 1-17 (2011).

15. E.O. Asare, A.M. Tompkins, A. Bomblies, A regional model for malaria vector developmental habitats evaluated using explicit, pond-resolving surface hydrology simulations. *PLoS One* **11**, p.e0150626 (2016).

16. J. Small, S.J. Goetz, S.I. Hay, Climatic suitability for malaria transmission in Africa, 1911–1995. *Proceedings of the National Academy of Sciences of the United States of America* **100**, 15341–15345 (2003).

17. M. Van Lieshout, R.S. Kovats, M.T.J. Livermore, P. Martens, Climate change and malaria: analysis of the SRES climate and socio-economic scenarios. *Global Environmental Change* **14**, 87-99 (2004).

18. C. Caminade, S. Kovats, J. Rocklov, A.M. Tompkins, A.P. Morse, F.J. Colón-González, H. Stenlund, P. Martens, S.J. Lloyd, Impact of climate change on global malaria distribution. *Proceedings of the National Academy of Sciences U.S.A.* **111**, 3286-3291 (2014).

19. F.J. Colón-González, M.O. Sewe, A.M. Tompkins, H. Sjödin, A. Casallas, J. Rocklöv, C. Caminade, R. Lowe, Projecting the risk of mosquito-borne diseases in a warmer and more populated world: a multi-model, multi-scenario intercomparison modelling study. *The Lancet Planetary Health* **5**, e404-e414 (2021).

20. M.W. Smith, T. Willis, L. Alfieri, W.H.M. James, M.A. Trigg, D. Yamazaki, A.J. Hardy, B. Bisselink, A. De Roo, M.G. Macklin, C.J. Thomas, Incorporating hydrology into climate suitability models changes projections of malaria transmission in Africa. *Nature Communications* **11**, p.4353 (2020).

21. C.E. Telteu, H. Müller Schmied, W. Thiery, G. Leng, P. Burek, X. Liu, J.E.S. Boulange, L.S. Andersen, M. Grillakis, S.N. Gosling, Y. Satoh, Understanding each other's models: an

introduction and a standard representation of 16 global water models to support intercomparison, improvement, and communication. *Geoscientific Model Development* **14**, 3843-3878 (2021).

22. K.L. Beven, N.A. Chappell, Perceptual perplexity and parameter parsimony. *Wiley Interdisciplinary Reviews: Water* **8**, p.e1530 (2021).

23. J.R. Thompson, S.N. Gosling, J. Zaherpour, C.L.R. Laizé, Increasing risk of ecological change to major rivers of the world with global warming. *Earth's Future* **9**, p.e2021EF002048 (2021).

24. A. Kumar, S.N. Gosling, M.F. Johnson, M.D. Jones, J. Zaherpour, R. Kumar, G. Leng, H.M. Schmied, J. Kupzig, L. Breuer, N. Hanasaki, Multi-model evaluation of catchment-and global-

scale hydrological model simulations of drought characteristics across eight large river catchments. *Advances in Water Resources* **165**, p.104212 (2022).

25. K. Frieler, S. Lange, F. Piontek, C.P. Reyer, J. Schewe, L. Warszawski, F. Zhao, L. Chini, S. Denvil, K. Emanuel, T. Geiger, Assessing the impacts of 1.5 C global warming simulation protocol of the Inter-Sectoral Impact Model Intercomparison Project (ISIMIP2b). *Geoscientific Model Development* **10**, 4321-4345 (2017).

26. Y.E. Himeidan, M.M. Elzaki, E.J. Kweka, M. Ibrahim, I.M. Elhassan, Pattern of malaria transmission along the Rahad River basin, Eastern Sudan. *Parasites & Vectors* **4**, 1-9 (2011).

27. M.E. Sinka, M.J. Bangs, S. Manguin, M. Coetzee, C.M. Mbogo, J. Hemingway, A.P. Patil, W.H. Temperley, P.W. Gething, C.W. Kabaria, R.M. Okara, The dominant *Anopheles* vectors of human malaria in Africa, Europe and the Middle East: occurrence data, distribution maps and bionomic précis. *Parasites & Vectors* **3**, 1-34 (2010).

28. A.J. Hardy, J.G.P. Gamarra, D.E. Cross, M.G. Macklin, M.W. Smith, J. Kihonda, G.F. Killeen, G.N. Ling'ala, C.J. Thomas, Habitat hydrology and geomorphology control the distribution of malaria vector larvae in rural Africa. *PLoS One* **8**, e81931 (2013).

29. D.E. Cross, C.J. Thomas, N. McKeown, V. Siaziyu, A. Healey, T. Willis, D. Singini, F. Liywalii, A. Silumesii, J. Sakala, M.W. Smith, M.G. Macklin, A.J. Hardy, P.W. Shaw,

Geographically extensive larval surveys reveal an unexpected scarcity of primary vector mosquitoes in a region of persistent malaria transmission in western Zambia. *Parasites & Vectors* **14**, 91 (2021).

30. D.E. Cross, A.J.E. Healey, N.J. McKeown, C.J. Thomas, N.A. Macarie, V. Siaziyu, D. Singini, F. Liywalii, J. Sakala, A. Silumesii, P.W. Shaw, Temporally consistent predominance

and distribution of secondary malaria vectors in the Anopheles community of the upper Zambezi floodplain. *Scientific Reports* **12**, 240 (2022).

31. M.E. Sinka, M.J. Bangs, S. Manguin, Y. Rubio-Palis, T. Chareonviriyaphap, M. Coetzee, C.M. Mbogo, J. Hemingway, A.P. Patil, W.H. Temperley, P.W. Gething, A global map of dominant malaria vectors. *Parasites & Vectors* **5**, 1-11 (2012).

32. A.J. Lysenko, I.N. Semashko, Geography of malaria. A medico-geographic profile of an ancient disease. *Itogi Nauki: Medicinskaja Geografija* **25**, 146 (1968).

33. A. Tabbabi, A.A. Alkishe, A.M. Samy, A. Rhim, A.T. Peterson, Malaria in north Africa: a review of the status of vectors and parasites. *Journal of Entomological Science* **55**, 25-37 (2020).

34. C. Skonieczny, P. Paillou, A. Bory, G. Bayon, L. Biscara, X. Crosta, F. Eynaud, B. Malaizé, M. Revel, N. Aleman, J.P. Barusseau, African humid periods triggered the reactivation of a large river system in Western Sahara. *Nature Communications* **6**, 8751 (2015).

35. M.A. Kenawy, Review of Anopheles mosquitoes and malaria in ancient and modern Egypt. *Journal of Mosquito Research* **5**, 1–8 (2015).

36. D. Kyalo, P. Amratia, C.W. Mundia, C.M. Mbogo, M. Coetzee, R.W. Snow, A geo-coded inventory of anophelines in the Afrotropical Region south of the Sahara: 1898-2016. *Wellcome Open Research* 2, 57 (2017).

37. S. Bhatt, D.J. Weiss, E. Cameron, D. Bisanzio, B. Mappin, U. Dalrymple, K.E. Battle, C.L. Moyes, A. Henry, P.A. Eckhoff, E.A. Wenger, The effect of malaria control on Plasmodium falciparum in Africa between 2000 and 2015. *Nature* 526, 207-211 (2015).

38. A. Wiebe, J. Longbottom, K. Gleave, F.M. Shearer, M.E. Sinka, N.C. Massey, E. Cameron, S. Bhatt, P.W. Gething, J. Hemingway, D.L. Smith, Geographical distributions of African

malaria vector sibling species and evidence for insecticide resistance. *Malaria Journal* 16, 1-10 (2017).

39. J. Leedale, A.M. Tompkins, C. Caminade, A.E. Jones, G. Nikulin, A.P. Morse, Projecting malaria hazard from climate change in eastern Africa using large ensembles to estimate uncertainty. *Geospatial Health* **11**, 102-114 (2016).

40. M.J. Pratt-Johnson, The distribution of malaria in South Africa and a mosquito survey of military hospital areas. *Epidemiology & Infection* **19**, 344-349 (1921).

41. B.J. Mafwele, J.W. Lee, Relationships between transmission of malaria in Africa and climate factors. *Scientific Reports* **12**, 14392 (2022).

42. J. Zaherpour, N. Mount, S.N. Gosling, R. Dankers, S. Eisner, D. Gerten, X. Liu, Y. Masaki, H.M. Schmied, Q. Tang, Y. Wada, Exploring the value of machine learning for weighted multi-

model combination of an ensemble of global hydrological models. *Environmental Modelling & Software* **114**, 112-128 (2019).

43. V. Krysanova, C. Donnelly, A. Gelfan, D. Gerten, B. Arheimer, F. Hattermann, Z.W. Kundzewicz, How the performance of hydrological models relates to credibility of projections under climate change. *Hydrological Sciences Journal* **63**, 696-720 (2018).

44. Y. Pokhrel, F. Felfelani, Y. Satoh, J. Boulange, P. Burek, A. Gädeke, D. Gerten, S.N. Gosling, M. Grillakis, L. Gudmundsson, N. Hanasaki, H. Kim, A. Koutroulis, J. Liu, L. Papadimitriou, J. Schewe, H. Müller Schmied, T. Stacke, C.-E. Telteu, W. Thiery, T. Veldkamp, F. Zhao, Y. Wada, Global terrestrial water storage and drought severity under climate change. *Nature Climate Change* **11**, 226-233 (2021).

45. L. Gudmundsson, J. Boulange, H.X. Do, S.N. Gosling, M.G. Grillakis, A.G. Koutroulis, M. Leonard, J. Liu, H. Müller Schmied, L. Papadimitriou, Y. Pokhrel, Globally observed trends in mean and extreme river flow attributed to climate change. *Science* **371**, 1159-1162 (2021).

46. M. Porkka, V. Virkki, L. Wang-Erlandsson, D. Gerten, T. Gleeson, C. Mohan, I. Fetzer, F. Jaramillo, A. Staal, S. te Wierik, A. Tobian, R. van der Ent, P. Döll, M. Flörke, S.N. Gosling, N. Hanasaki, Y. Satoh, H. Müller Schmied, N. Wanders, J.S. Famiglietti, J. Rockström, M. Kummu,

Notable shifts beyond pre-industrial streamflow and soil moisture conditions transgress the planetary boundary for freshwater change. *Nature Water* **2**, 1-12 (2024).

47. I. Diouf, A.M. Adeola, G.J. Abiodun, C. Lennard, J.M. Shirinde, P. Yaka, J.A. Ndione, E.O. Gbobaniyi, Impact of future climate change on malaria in West Africa. *Theoretical and Applied Climatology* **147**, 853–865 (2022).

48. C.H. Trisos, I.O. Adelekan, E. Totin, A. Ayanlade, J. Efitre, A. Gemeda, K. Kalaba, C. Lennard, C. Masao, Y. Mgaya, G. Ngaruiya, D. Olago, N.P. Simpson, S. Zakieldeen, "Chapter 9 Africa" in *Climate Change 2022: Impacts, Adaptation and Vulnerability*. (IPCC, 2022), pp. 1285–1455.

49. E.A. Mordecai, S.J. Ryan, J.M. Caldwell, M.M. Shah, A.D. LaBeaud, Climate change could shift disease burden from malaria to arboviruses in Africa. *The Lancet Planetary Health* **4**, e416-e423 (2020).

50. S.N. Gosling, H.M. Schmied, P. Burek, J. Chang, P. Ciais, P. Döll, S. Eisner, G. Fink, M. Flörke, W. Franssen, M. Grillakis, S. Hagemann, N. Hanasaki, A. Koutroulis, G. Leng, X. Liu, Y. Masaki, C. Mathison, V. Mishra, S. Ostberg, F. Portmann, W. Qi, R.-K. Sahu, Y. Satoh, J. Schewe, S. Seneviratne, H.L. Shah, T. Stacke, F. Tao, C. Telteu, W. Thiery, T. Trautmann, I. Tsanis, N. Wanders, R. Zhai, M. Büchner, J. Schewe, F. Zhao, ISIMIP2b Simulation Data from

the Global Water Sector, version 1.0. ISIMIP Repository (2023);
https://doi.org/10.48364/ISIMIP.626689

51. WorldPop and Center for International Earth Science Information Network (CIESIN), Columbia University (2020). Global High Resolution Population Denominators Project (OPP1134076) (2020); https://dx.doi.org/10.5258/SOTON/WP00647.

52. United Nations, Department of Economic and Social Affairs, Population Division, "World Population Prospects 2022" (United Nations, 2022); https://population.un.org/wpp/.

53. M.W. Smith, T. Willis, E. Mroz, W.H.M. James, M.J. Klaar, S.N. Gosling, C.J. Thomas, Estimates of hydro-climatic suitability for malaria transmission in Africa (2024); https://doi.org/10.5518/1415

54. S. Lange, M. Büchner, ISIMIP2b bias-adjusted atmospheric climate input data, version 1.0, ISIMIP Repository (2017); https://doi.org/10.48364/ISIMIP.208515.

55. S. Lange, Bias correction of surface downwelling longwave and shortwave radiation for the EWEMBI dataset. *Earth System Dynamics* **9**, 627-645 (2018).

56. W. Thiery, E.L. Davin, D.M. Lawrence, A.L. Hirsch, M. Hauser, S.I. Seneviratne, Present-day irrigation mitigates heat extremes. *Journal of Geophysical Research: Atmospheres* **122**, 1403-1422 (2017).

57. N. Hanasaki, S. Yoshikawa, Y. Pokhrel, S. Kanae, A global hydrological simulation to specify the sources of water used by humans. *Hydrology and Earth System Sciences* **22**, 789-817 (2018).

58. S. Sitch, B. Smith, I.C. Prentice, A. Arneth, A. Bondeau, W. Cramer, J.O. Kaplan, S. Levis, W. Lucht, M.T. Sykes, K. Thonicke, Evaluation of ecosystem dynamics, plant geography and

terrestrial carbon cycling in the LPJ dynamic global vegetation model. *Global Change Biology* **9**, 161-185 (2003).

59. T. Stacke, S. Hagemann, Development and evaluation of a global dynamical wetlands extent scheme. *Hydrology and Earth System Sciences* **16**, 2915-2933 (2012).

60. M. Guimberteau, A. Ducharne, P. Ciais, J.P. Boisier, S. Peng, M. De Weirdt, H. Verbeeck, Testing conceptual and physically based soil hydrology schemes against observations for the Amazon Basin. *Geoscientific Model Development* **7**, 1115-1136 (2014).

61. E.H. Sutanudjaja, R. Van Beek, N. Wanders, Y. Wada, J.H. Bosmans, N. Drost, R.J. Van Der Ent, I.E. De Graaf, J.M. Hoch, K. De Jong, D. Karssenberg, PCR-GLOBWB 2: a 5 arcmin global hydrological and water resources model. *Geoscientific Model Development* **11**, 2429-2453 (2018).

62. H. Müller Schmied, L. Adam, S. Eisner, G. Fink, M. Flörke, H. Kim, T. Oki, F.T. Portmann, R. Reinecke, C. Riedel, Q. Song, Variations of global and continental water balance components as impacted by climate forcing uncertainty and human water use. *Hydrology and Earth System Sciences* **20**, 2877-2898 (2016).

63. R. Wartenburger, S.I. Seneviratne, M. Hirschi, J. Chang, P. Ciais, D. Deryng, J. Elliott, C. Folberth, S.N. Gosling, L. Gudmundsson, A. Henrot, T. Hickler, A. Ito, N. Khabarov, H. Kim,

G. Leng, J. Liu, X. Liu, Y. Masaki, C. Morfopoulos, C. Müller, H.M. Schmied, K. Nishina, R. Orth, Y.N. Pokhrel, T. Pugh, Y. Satoh, S. Schaphoff, E. Schmid, J. Sheffield, T. Stacke, J. Steinkamp, Q. Tang, W. Thiery, Y. Wada, X. Wang, G.P. Weedon, H. Yang, T. Zhou, Evapotranspiration simulations in ISIMIP2a - Evaluation of spatio-temporal characteristics with a comprehensive ensemble of independent datasets. *Environmental Research Letters* **13**, 075001 (2018).

64. J. Zaherpour, S.N. Gosling, N. Mount, H.M. Schmied, T.I.E. Veldkamp, R. Dankers, S. Eisner, D. Gerten, L. Gudmundsson, I. Haddeland, N. Hanasaki, H. Kim, G. Leng, J. Liu, Y. Masaki, T. Oki, Y.N. Pokhrel, Y. Satoh, J. Schewe, Y. Wada, Worldwide evaluation of mean

and extreme runoff from six global-scale hydrological models that account for human impacts. *Environmental Research Letters* **13**, 065015 (2018).

65. F. Tanser, B.L. Sharp, D. Le Sueur, Potential effect of climate change on malaria transmission in Africa. *The Lancet* **362**, 1792–9178 (2003).

66. K.P. Paaijmans, W. Takken, A.K. Githeko, A.F.G. Jacobs, The effect of water turbidity on the near-surface water temperature of larval habitats of the malaria mosquito *Anopheles gambiae*. *International Journal of Biometeorology* **52**, 747–753 (2008).

67. T.K. Yamana, E.A. Eltahir, Incorporating the effects of humidity in a mechanistic model of *Anopheles gambiae* mosquito population dynamics in the Sahel region of Africa. *Parasites & Vectors* **6**, 1-10 (2013).

68. S.W. Lindsay, L. Parson, C.J. Thomas, Mapping the ranges and relative abundance of the two principal African malaria vectors, *Anopheles gambiae* sensu stricto and *An. arabiensis*, using climate data. *Proceedings of the Royal Society B: Biological Sciences* **265**, 847–854 (1998).

69. R. Reinecke, H. Müller Schmied, T. Trautmann, L.S. Andersen, P. Burek, M. Flörke, S.N. Gosling, M. Grillakis, N. Hanasaki, A. Koutroulis, Y. Pokhrel, Uncertainty of simulated

groundwater recharge at different global warming levels: a global-scale multi-model ensemble study. *Hydrology and Earth System Sciences* **25**, 787-810 (2021).

70. P. Reiter, Global warming and malaria: knowing the horse before hitching the cart. *Malaria Journal* **7**, S3 (2008).

71. D. Wilks, *Statistical Methods in the Atmospheric Sciences* (Elsevier, 2006).

72. E. Stephens G. Schumann, P. Bates, Problems with binary pattern measures for flood model evaluation. *Hydrological Processes* **28**, 4928–37 (2014).

73. M.V. Bernhofen, C. Whyman, M.A. Trigg, P.A. Sleigh, A.M. Smith, C.C. Sampson, D. Yamazaki, P.J. Ward, R. Rudari, F. Pappenberger, F. Dottori, A first collective validation of

global fluvial flood models for major floods in Nigeria and Mozambique. *Environmental Research Letters* **13**, p.104007 (2018).

74. A. Chemison, G. Ramstein, A.M. Tompkins, D. Defrance, G. Camus, M. Charra, C. Caminade, Impact of an accelerated melting of Greenland on malaria distribution over Africa. *Nature Communications* **12**, 3971 (2021).

75. P. Martens, P., R.S. Kovats, S. Nijhof, P. De Vries, M.T.J. Livermore, D.J. Bradley, J. Cox, A.J. McMichael, Climate change and future populations at risk of malaria. *Global Environmental Change* **9**, S89–S107 (1999).

76. K.A. Smith, R.L. Wilby, C. Broderick, C. Prudhomme, T. Matthews, S. Harrigan, C. Murphy, Navigating Cascades of Uncertainty — As Easy as ABC? Not Quite…. *Journal of Extreme Events* **5**, 1850007.

77. C. Pezzulo, K. Nilsen, A. Carioli, N. Tejedor-Garavito, S.E. Hanspal, T. Hilber, W.H. James, C.W. Ruktanonchai, V. Alegana, A. Sorichetta, A.S. Wigley, Geographical distribution of fertility rates in 70 low-income, lower-middle-income, and upper-middle-income countries,

2010–16: a subnational analysis of cross-sectional surveys. *The Lancet Global Health* **9**, e802–e812 (2021).

78. W.H. James, N. Tejedor-Garavito, S.E. Hanspal, A. Campbell-Sutton, G.M. Hornby, C. Pezzulo, K. Nilsen, A. Sorichetta, C.W. Ruktanonchai, A. Carioli, D. Kerr, Gridded birth and pregnancy datasets for Africa, Latin America and the Caribbean. *Scientific Data* **5**, 1-11 (2018).

Acknowledgments: We thank those involved in the ISIMIP project for making the model data available.

Funding: This work was undertaken with support from the UK Natural Environment Research Council (NERC) award FLOODMAL (NE/P013481/1) (MWS and CJT), and Leeds-York-Hull NERC Doctoral Training Partnership (NE/S007458/1) (EM). This paper is also based upon work undertaken as part of COST Action PROCLIAS, supported by COST (European Cooperation in Science and Technology), www.cost.eu.

Author contributions:

Conceptualization: MWS and CJT

Study design and methods: MWS with support from SNG

Data processing: MWS, TW and W.H.M.J.

Data analysis: MWS, EM, MJK and WHMJ

Writing initial draft: MWS

Writing review and editing: all authors.

Competing interests: Authors declare that they have no competing interests.

Data and materials availability: Global Climate Model data (*40*) and Global Hydrological Model data (*50*) used in this study are available via the ISIMIP Repository. Population grids (total and age-structured) are available to download from the WorldPop dataset (*51*). UN country level population estimates and projections (total and age-structured) are available to download from the United Nations, Department of Economic and Social Affairs (*52*). Malaria suitability estimates from this paper and source data for figures are available for download from the Research Data Leeds Repository (*53*).

Supplementary Materials

Materials and Methods

Figs. S1 – S16

Tables S1 – S11

References (54 – 78)

Figure Captions

Fig. 1. Variability in malaria hydro-climatic suitability estimates (1986-2005). (**A**) Mean Length of Transmission Season (LTS, in months) estimates for each hydrological representation (mean of all GCM and GHM combinations). (**B**) Model agreement across each ensemble. Maps indicate the percentage of models in the ensemble that estimate LTS > 6 months (full data presented in Fig. S1 and Table S1). (**C**) LTS estimates for each hydrological representation calculated within 3-month bands using the model ensemble weightings established in later validation. (**D**-**F**) Estimates of seasonal (LTS > 6 months) and endemic malaria suitability (LTS > 9 months) showing all individual model estimates across different hydrological models (bars showing mean value) and global climate models (individual points for each climate model, n = 4). Precipitation is plotted separately in (D). (**G**) Variance ratios for all hydrology-derived layers showing the percentage of variance in malaria LTS contributed by GCMs for each model cell.

Fig. 2. Validation of model hydroclimatic malaria suitability estimates. (**A**) Pre-intervention malaria map of Lysenko and Semashko (*32*); (**B**) weighted ensemble model estimates of hydro-climatic malaria suitability LTS (1875-1900); (**C**-**D**) summary of ensemble validation metrics for each hydrological representation, with both metrics plotted separately and combined as an ensemble score (full data in Tables S2-S3); (**E**) estimates of malaria suitability by the weighted ensembles for each hydrological representation calculated within 3-month bands; (**F**) selected validation maps comparing observed and modelled malaria suitability (where at least one month

is suitable). Figs. S6-S9 present validation maps and LTS maps for all hydrological representations.

Fig. 3. Future projections of malaria hydro-climatic suitability. (**A**, **E**) Projected Length of Transmission Season in RCP 8.5 for 2076-2100. Areas showing an increase or decrease in suitability since 1986-2005 across all scenarios and time periods are plotted in (**B**, **F**) showing only areas with a signal-to-noise ratio (SNR) > 0.5. The locations of these changing areas are shown for RCP 8.5 (2076-2100) in (**C**, **G**) and for all RCP scenarios and time periods in Fig. S11. The extent of change in suitability (number of months change) is plotted by signal-to-noise ratio as stacked histograms for RCP 8.5 in (**D**, **H**) and for all scenarios in Fig. S12.

Fig. 4. Future populations in areas hydro-climatically suitable for malaria transmission. (**A**) Populations within 3-month bands of LTS for both precipitation and discharge with potential evapotranspiration hydrological representations. Bars show total populations for each RCP for each weighted ensemble. Points indicate population under-5 years old. Populations calculated using UN medium variant projections for each period. (**B**) Predicted percentage changes in population-months (i.e., population exposed multiplied by the number of additional months of exposure) since 1986-2005 by country for RCP 8.5 only (see Fig. S13 for each RCP). White indicates no estimated malaria suitability.

Submitted Manuscript: Confidential
Template revised November 2022

Supplementary Materials for

Future malaria environmental suitability in Africa is sensitive to hydrology

Mark W. Smith*, Thomas Willis, Elizabeth Mroz, William H. M. James, Megan J. Klaar, Simon N. Gosling, Christopher J. Thomas

Corresponding author: m.w.smith@leeds.ac.uk

The PDF file includes:

Materials and Methods
Figs. S1 to S14
Tables S1 to S10
References (54 – 78)

Materials and Methods

Climate data

Climate data were downloaded for four Global Climate Models (GCMs) (GFDL-ESM2M, HadGem2-ES, IPSL-CM5A-LR and MIROC-ESM-CHEM) for three RCPs (RCP 2.6, RCP 6.0 and RCP 8.5) chosen to represent a range of radiative forcings and uncertainty regarding future greenhouse gas emissions. These data were retrieved from the database of the Inter-Sectoral Impact Model Intercomparison Project (ISIMIP2b) (*25*, *54*). All climate variables were obtained on a latitude-longitude grid of 0.5 x 0.5 degrees covering the extent of Africa. Climate variables comprised of bias-adjusted (*25*, *55*) daily mean surface temperature (in K), daily total precipitation (in kg m^{-2} s^{-1}), and daily relative humidity (in %). Historical daily climate data were downloaded for the period 1986-2005; future climate simulations for each RCP were split into four periods: 2006-2025 (to represent present conditions), 2026-2050, 2051-2075 and 2076-2100.

Hydrological modelling

Climate data from each combination of GCM and RCP were used to drive seven global hydrological models on a daily time step. Global hydrological models included were CLM45 (*56*), H08 (*57*), LPJml (*58*), MPI-HM (*59*), ORCHIDEE (*60*), PCR-GLOBW (*61*) and WaterGAP2-2c (*62*). The GHMs represent an ensemble of opportunity and while some models use similar methods to represent some hydrological processes, there are many differences in the ways that the models parameterize others (*21*). The differences in LTS between LPJmL and ORCHIDEE (Fig. S2) reflect these model differences. The different approaches for calculating potential evapotranspiration between GHMs often explains some of the differences between the ISIMIP2b GHM simulations of runoff (*63*, *64*), for example, ORCHIDEE applies a simplified Penman–Monteith equation whereas LPJmL applies the Priestley–Taylor equation (*21*). While historical society scenarios were used to model human influences on hydrology (e.g., land use and irrigation) for the preindustrial and historical model runs (*25*), 2005 society models were used for all future estimates to isolate the climate change signal. Daily modelled discharge (m^3 s^{-1}) and monthly modelled potential evapotranspiration (both in kg m^{-2} s^{-1}) output from GHMs were used as variables to represent hydrological malaria suitability. These data were available via the ISIMIP2b database.

Estimation of malaria hydrological suitability

Average daily surface temperature, relative humidity, discharge, potential evapotranspiration and total precipitation were calculated for each month. For each combination of GCM and GHM, six methods of estimating hydrological suitability for malaria transmission were calculated based on monthly values of climate and hydrological parameters averaged across each of the above time periods.

(i) Precipitation (PR): the 60 mm monthly precipitation threshold of Tanser et al. (*65*) was implemented, including the requirement of a catalyst 80 mm month (i.e., a single month where precipitation exceeds 80 mm).

(ii) Discharge (Q): a minimum of 1 mm depth across the grid cell was used as a threshold for daily hydrological model discharge output, indicating sufficient water availability (equating to approximately 30 m^3 s^{-1}). Previous sensitivity analysis (*20*) indicated limited sensitivity of hydro-climatic malaria suitability estimates to this value, particularly when compared to the sensitivity of precipitation thresholds. The number of days this condition is met per month was

then averaged for each time period; when this exceeded the temperature-dependent development period of *Anopheles* mosquitoes (calculated using the model of Bayoh and Lindsay (*10*)), the month was deemed to be hydrologically suitable for malaria transmission. As per Smith et al. (*20*), the average daily mean surface air temperature was used to establish the development rate to maturity, though where this is below the 31 °C optimum water temperature, we apply a +2 °C offset as suggested by Paaijmans et al. (*66*) to account for the typical difference observed between surface air temperature and water temperature. Since shading is often available, we do not apply this offset for temperatures above the optimum as larvae are likely to seek optimum conditions where available.

(iii) Discharge with relative humidity (Q_RH): an additional criterion was imposed on the discharge estimates of a minimum relative humidity of 40% (*67*).

(iv) Potential evapotranspiration (PE): the ratio of total precipitation and potential evapotranspiration was calculated and following Lindsay et al. (*68*) a minimum value of 0.5 was considered suitable for malaria transmission.

(v) Discharge with potential evapotranspiration (Q_PE): a union of the discharge and potential evapotranspiration suitability layers was computed as the most physically realistic of representing locally-generated surface water alongside larger discharge transfers. Combining suitability layers in this way avoids any double-counting of water in the hydrological model outputs.

(vi) Discharge with potential evapotranspiration and relative humidity (Q_PE_RH): the relative humidity criterion was also applied to (v).

All data were transformed into an equal area projection (Africa Albers Equal Area Conic) appropriate for calculation of areas of malaria transmission over the African continent.

Hydro-climatic suitability and model metrics

We combine our hydrological suitability layers with the temperature curve of Mordecai et al. (*8*). Following (*17*) and given our focus on hydro-climatic suitability, the full range of viable temperatures (16-34°C) is considered suitable. The temperature suitability was then combined with each hydrological suitability layer to create a monthly mask of hydro-climatically suitable areas for malaria suitability. The Length of Transmission Season (LTS) was then determined as the maximum number of continuous months of hydro-climatic suitability. Subsequent data analysis was undertaken in Stata 12.1.

Calculation of Model Variance

To calculate whether the variance in estimated malaria suitability is introduced primarily through GCMs or GHMs, the variance ratio (R_{var}) of GCMs to GHMs was calculated (*69*). For each grid cell, the average variance in malaria LTS for all GCMs (σ^2_{GCM}) and the average variance in malaria LTS for all GHMs (σ^2_{GHM}) are computed and the variance ratio calculated as

$$R_{var} = \frac{\sigma^2_{GCM}}{\sigma^2_{GCM} + \sigma^2_{GHM}}. \quad \text{(Equ. 1)}$$

To provide an overall metric of the source of variance, Equ. 1 was also applied to model estimates of areas of stable (>3 months), seasonal (>6 months) and endemic (>9 months) malaria transmission and all suitable areas (>1 month).

Model Validation and Ensemble Creation

Estimates of hydro-climatic suitability for malaria transmission are challenging to evaluate quantitatively, as there are numerous non-climatic controls on malaria transmission (*70*) including the successful reduction in transmission ranges due to interventions over the last century (*3*). For this reason, we focus our validation efforts on the pre-intervention map of Lysenko and Semashko (*32*) which is an approximation of malaria extents at ~1900AD, though the exact boundaries should be viewed with caution. ISIMIP2b climate and hydrological data were extracted for the years 1875-1900 and malaria hydro-climatic suitability calculated. Preindustrial climate and CO_2 scenarios were used where available; only 1986-2005 were available for ORCHIDEE (the differences and possible effects are demonstrated in Fig. S3). Two validation metrics are used: the most comprehensive performance score is the F^2 score (*71*) calculated from observed (F_o) and modelled (F_m) extents as

$$F^2 = \frac{F_m \cap F_o}{F_m \cup F_0}, \quad \text{(Equ. 2)}$$

where $F_m \cap F_o$ is the intersection of modelled and observed malaria suitability extent (i.e. correct forecasts) and $F_m \cup F_o$ is the union of modelled and observed extents. Since the F^2 score is biased towards overprediction (72), we follow Bernhofen et al. (*73*) in also calculating the bias metric (*71*) which measures whether an estimate is biased towards underprediction (negative bias score) or overprediction (positive) calculated as

$$Bias = \frac{(F_m \cap F_o) + F_m}{(F_m \cap F_o) + F_o} - 1. \quad \text{(Equ. 3)}$$

The performance of each individual model on each of these metrics is shown in Fig. S4. Finally, following (*73*) a single Ensemble Score (*ES*) was calculated as

$$ES = Average\ F^2 - |0.2 * Average\ Bias|, \quad \text{(Equ. 4)}$$

where the bias adjustment factor of 0.2 was selected to penalise for bias while still weighting F^2 as the most important score. ES was calculated for all hydro-climatic layers at two malaria LTS levels: >1 month (i.e., all malaria suitability) or >3 months continuous transmission suitability to indicate meso-endemicity, following Chemison et al. (*74*) and Martens et al. (*75*) (Tables S2-S3).

ES was used to weight all models within the ensemble (i.e., all combinations of global climate models and hydrological models for each hydro-climatic suitability layer). Weights from unity-based normalisation (scaled 0-1) were awarded to each model separately for each malaria level. Finally, model agreement layers (i.e., minimum number of models in the ensemble agreeing that malaria transmission is suitable at a given location) were created for all agreement levels (ranging from a layer showing where at least one model identified suitability to a layer showing only where all models in the ensemble agreed was suitable for malaria). Each of these agreement layers was validated based on ES (Fig. S5). The optimum number of model agreements for each hydro-climatic suitability layer was calculated (see Table S4) and that number of the top performing models in each ensemble were then awarded a maximum weight (*73*). The weights for all and meso-endemic malaria levels were merged and then renormalized such that the total weights in each ensemble are 1 (Fig. S6 and Table S5). These ensemble weights were then used to make future predictions using the model ensembles, noting that some rescaling is needed for RCP 8.5 where MPI-HM and PCR-GLOWB hydrological model outputs were unavailable. This ensemble approach is common practice and allows for a representation of the range of possible

outcomes across the models used. However, the cascade of uncertainty that prevails in climate change impact assessment (*76*), means that even with model intercomparison projects like ISIMIP and CMIP, it is impossible to analyse the full range of uncertainty because such projects are not exhaustive in their selection of models and scenarios.

Further validation of the final weighted layers was performed for each hydrological representation using the historical time period (1986-2005). The anopheles inventory for sub-Saharan Africa (1898-2016) of Kyalo et al. (*36*) is independent of climate but provides only a discontinuous distribution of observation locations. Given this limitation and the more reduced range of contemporary malaria and anopheles prevalence, the percentage of positive observations that are correctly modelled was calculated as the most appropriate metric (Table S6). We also compare model predictions with both malaria parasite ratio data from the Malaria Atlas Project (considering areas where the parasite ratio >0.01% in the year 2000 (*37*)) and the estimate of the mean modelled relative probability of occurrence of *Anopheles gambiae* (considering areas where the probability >0.05) of Wiebe et al. (*38*) (Fig. S9). However, it should be noted that both these datasets rely in some part on gridded climate data for interpolation and do not therefore serve for validation analysis independent of climate.

Population data

Human population analysis was carried out using the methodology outlined in Smith et al. (*20*). Gridded estimates of the human population in Africa were provided by WorldPop (*51*) at a resolution of 30 arc seconds (~1 km at the equator). These were used to evaluate the number of individuals residing within areas climatically suitable for malaria transmission. Analysis was performed for individuals of all ages and for children aged under five years of age as this group is particularly susceptible to malaria (*77*, *78*). Analysis was performed for the mid-point of each time period using the closest WorldPop grids (available annually between 2000 and 2020). For past and contemporary scenarios, grids were rescaled to match country level UN estimates (total population and under 5s) at the mid-point year of each time period (*52*). A similar approach was used for future scenarios, using country level UN projections (*52*) to maintain consistency with estimates for the historical periods. Primary analysis was based on the UN medium projection variant, whilst supplementary analysis was performed using the UN low and high projection variants for comparison and sensitivity analysis. Final results were aggregated to the continental and country level.

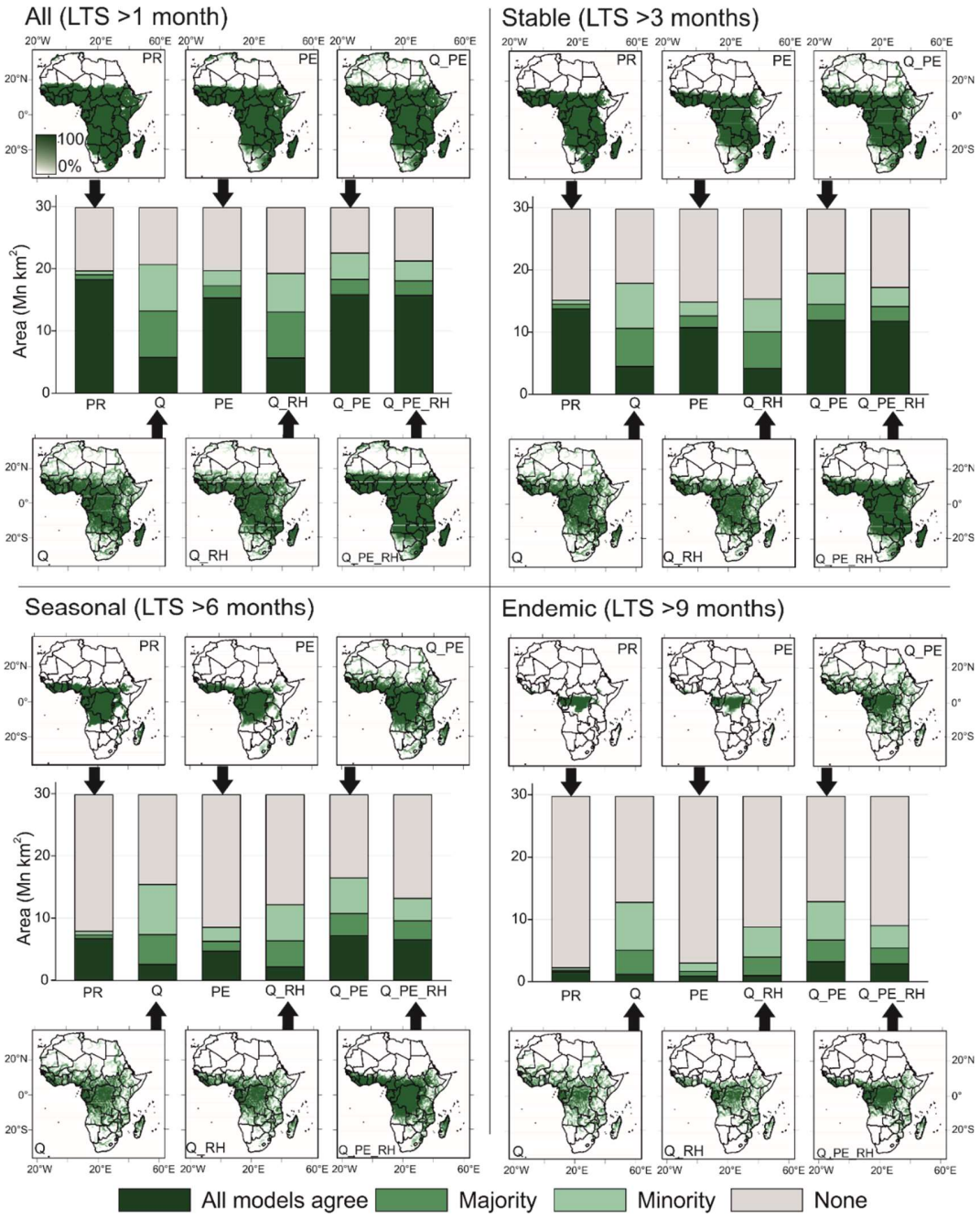

Fig. S1.

Areas of different levels of model agreement for model ensembles for each hydrological representation (areas stated in Mn km^2) and four malaria season length classifications: 'All' (LTS >1 month), 'Stable' (LTS > 3 months), 'Seasonal' (LTS > 6 months) and 'Endemic' (LTS > 9 months). Maps show the percentage of models in each ensemble that agree malaria is present to at least each transmission level. Note the different ensemble sizes for each hydrological representation (Table S1).

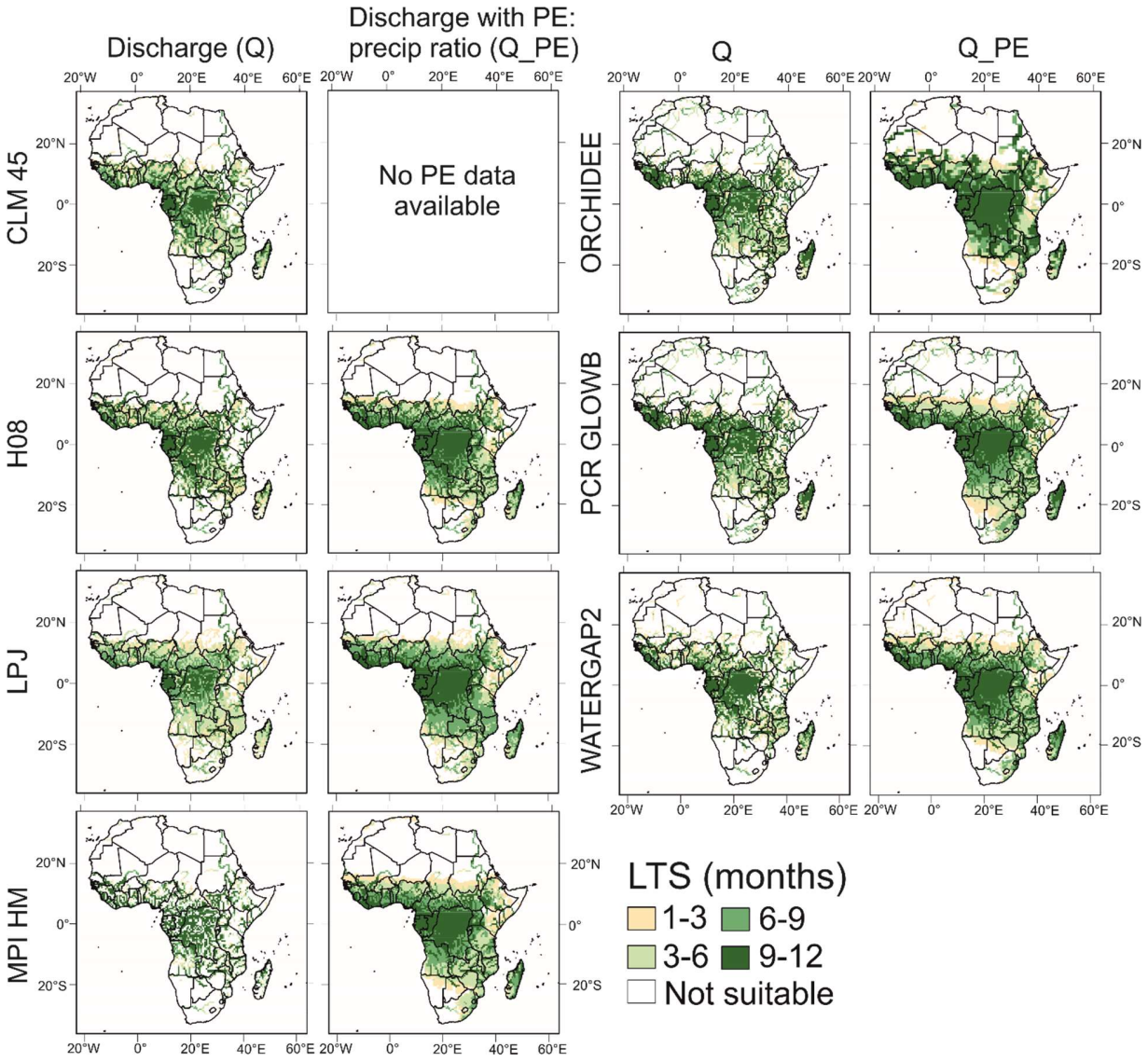

Fig. S2.

Comparison of historical (1986-2005) malaria length of transmission season (LTS) estimates for each hydrological model, for both 'discharge' and 'discharge with potential evapotranspiration' hydrological representations. LTS estimates are averages across the four global climate models.

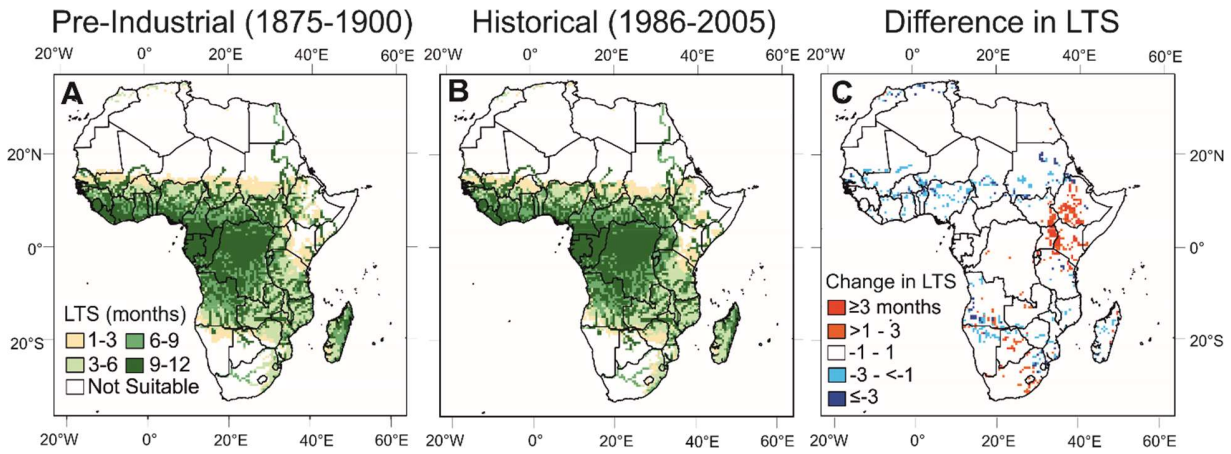

Fig. S3.

Example difference in LTS of malaria transmission hydro-climatic suitability for validation layers (Q_PE hydrological representation, IPSL GCM, H08 hydrological model). Pre-Industrial society (1875-1900) (**A**) is used for model validation; however, due to data availability, ORCHIDEE hydrological models use 1986-2005 data (**B**) as an approximation. (**C**) Shows the changes in LTS estimates since the preindustrial period (i.e., historical – preindustrial) where red shades indicate an extension of the transmission season.

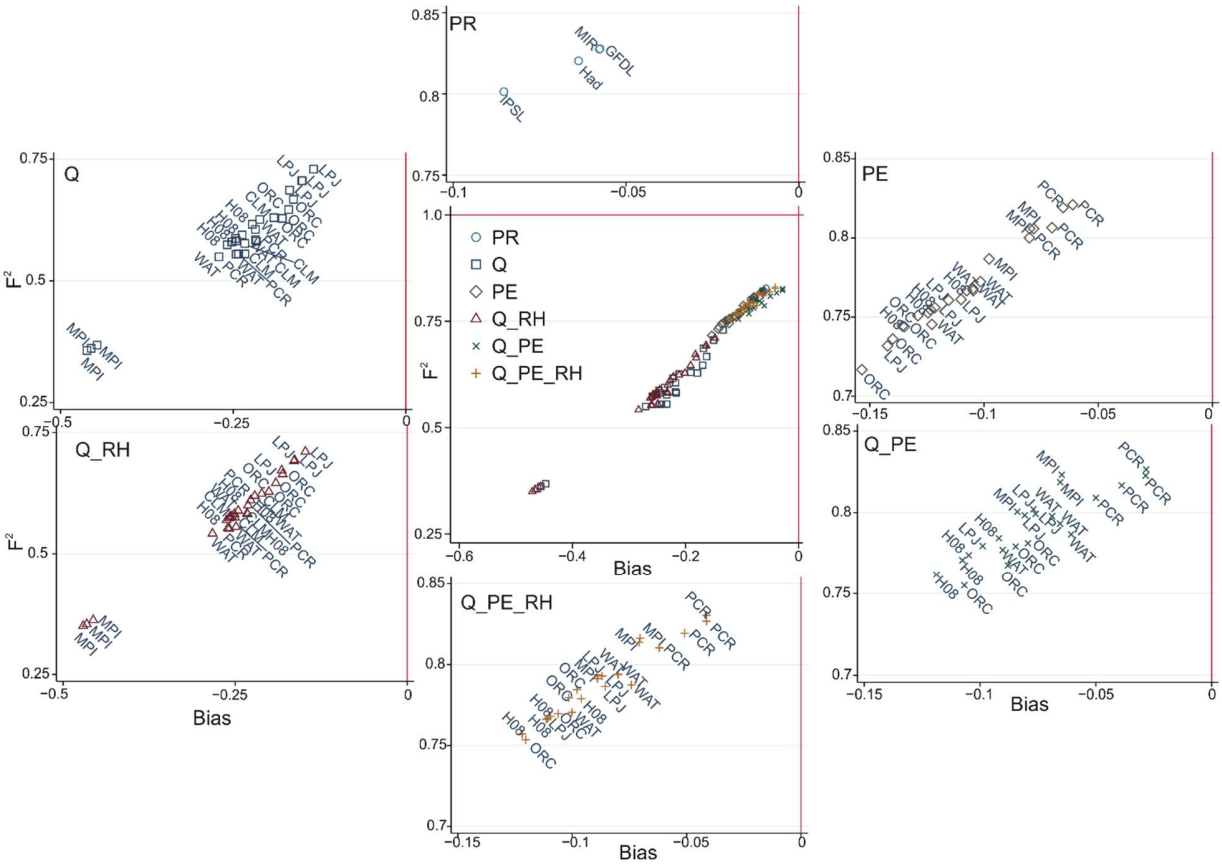

Fig. S4.

Validation metrics of model performance (F^2 and Bias) for all models in each ensemble (shown here for the >1 month malaria suitability level). The central panel shows all ensembles together, while those around the periphery separate these by hydrological representations and labels for each point indicate the hydrological model (or GCM for precipitation models).

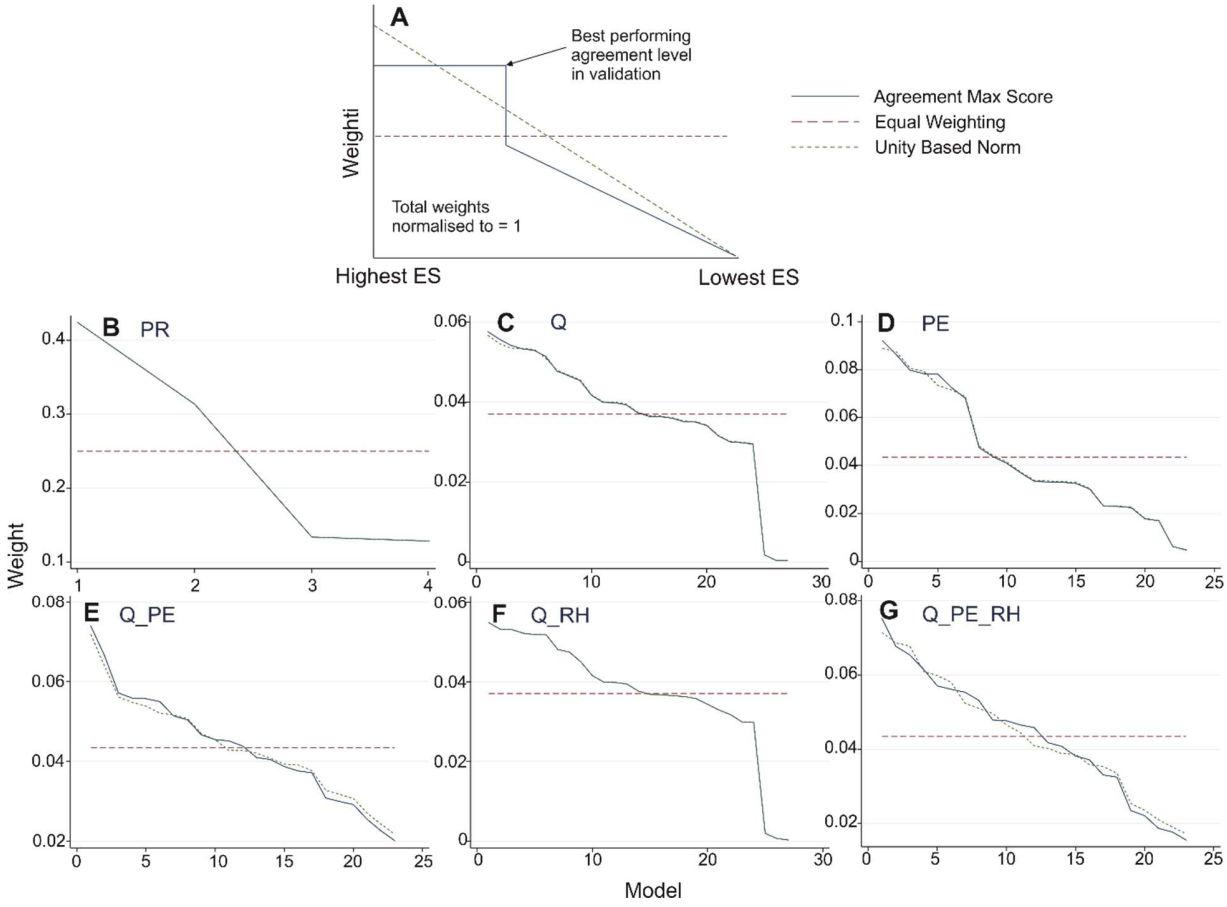

Fig. S5.

Weighting curves applied to each model ensemble based on validation performance. (**A**) Schematic of weighting curve calculation. Ensemble score (ES) is used to rank each model and a unity-based normalisation used to assign a weight. The best models up to the best-performing number of model agreements are then assigned a maximum weighting, with weights calculated separately for 'all malaria' and >mesoendemic season length (>3 months). These are summed and rescaled to 1. Models are ordered from best performing (left) to worst performing (right). (**B-G**) Weights are shown for ensembles for each hydrological representation.

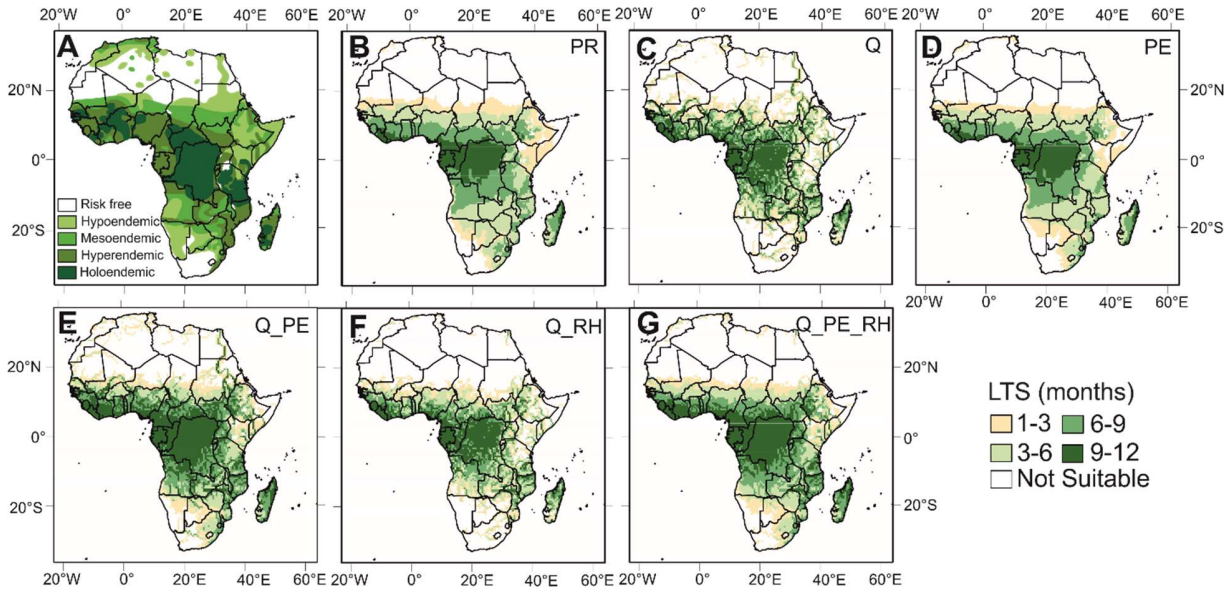

Fig. S6.

Malaria season length maps (1875-1900) for each hydrological representation model ensemble. Fig. 2E displays the areas by 3-month wide classification.

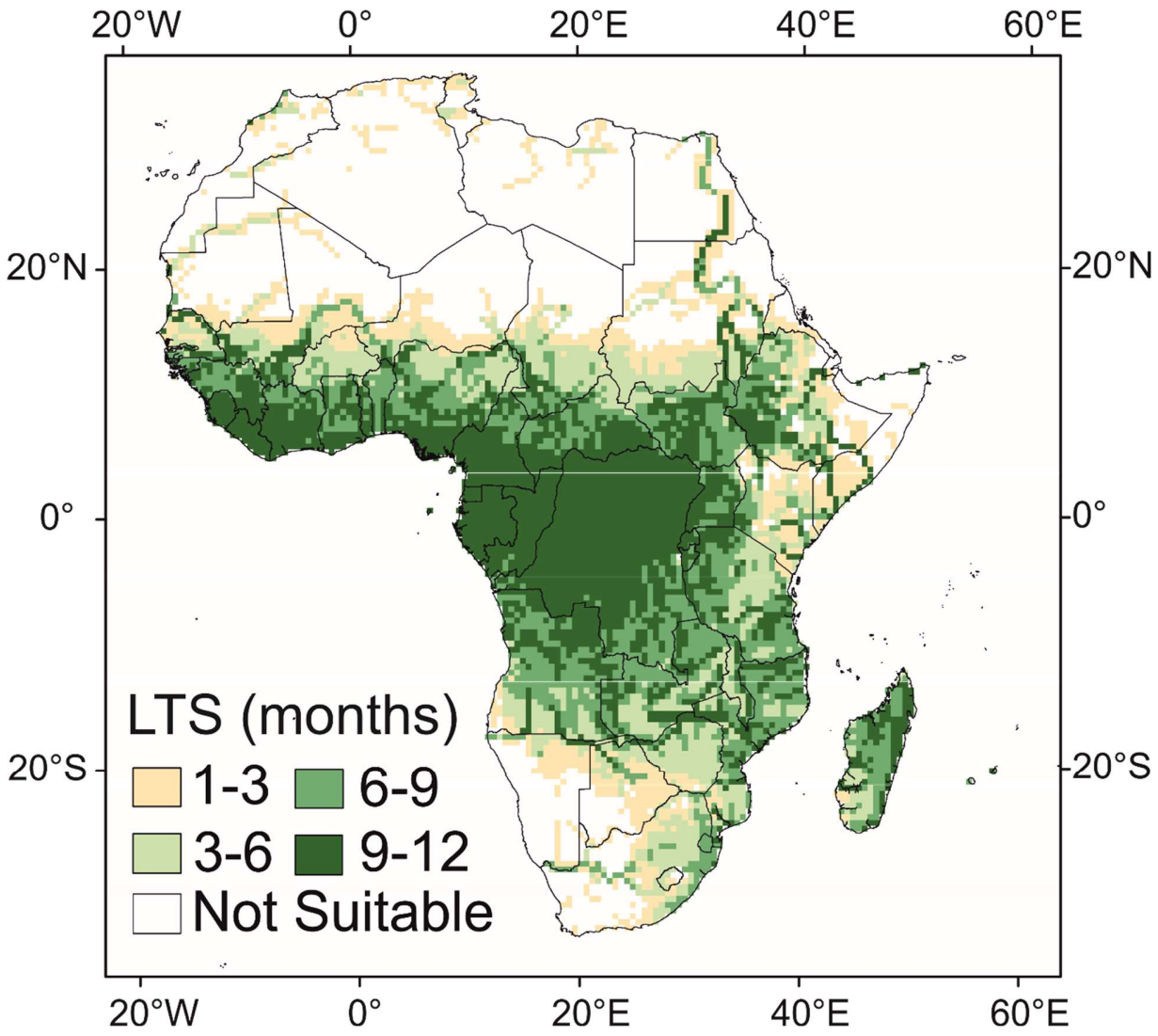

Fig. S7.

An enlarged version of the malaria season length predictions from the weighted ensemble of hydrologically-informed (Q_PE) malaria season length models for the historical period (1986-2005) for each hydrological representation model ensemble.

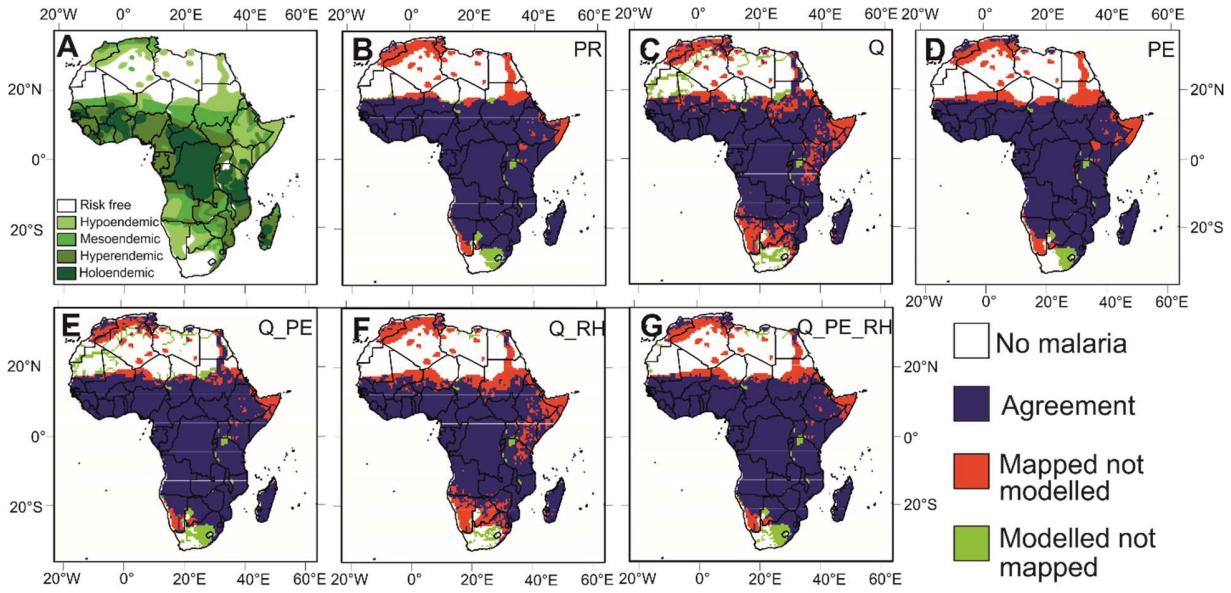

Fig. S8.

Validation layers for final weighted ensembles for each hydrological representation. The Lysenko and Semashko (*32*) pre-intervention malaria map is compared against model estimates for 1875-1900 with a pre-industrial society model.

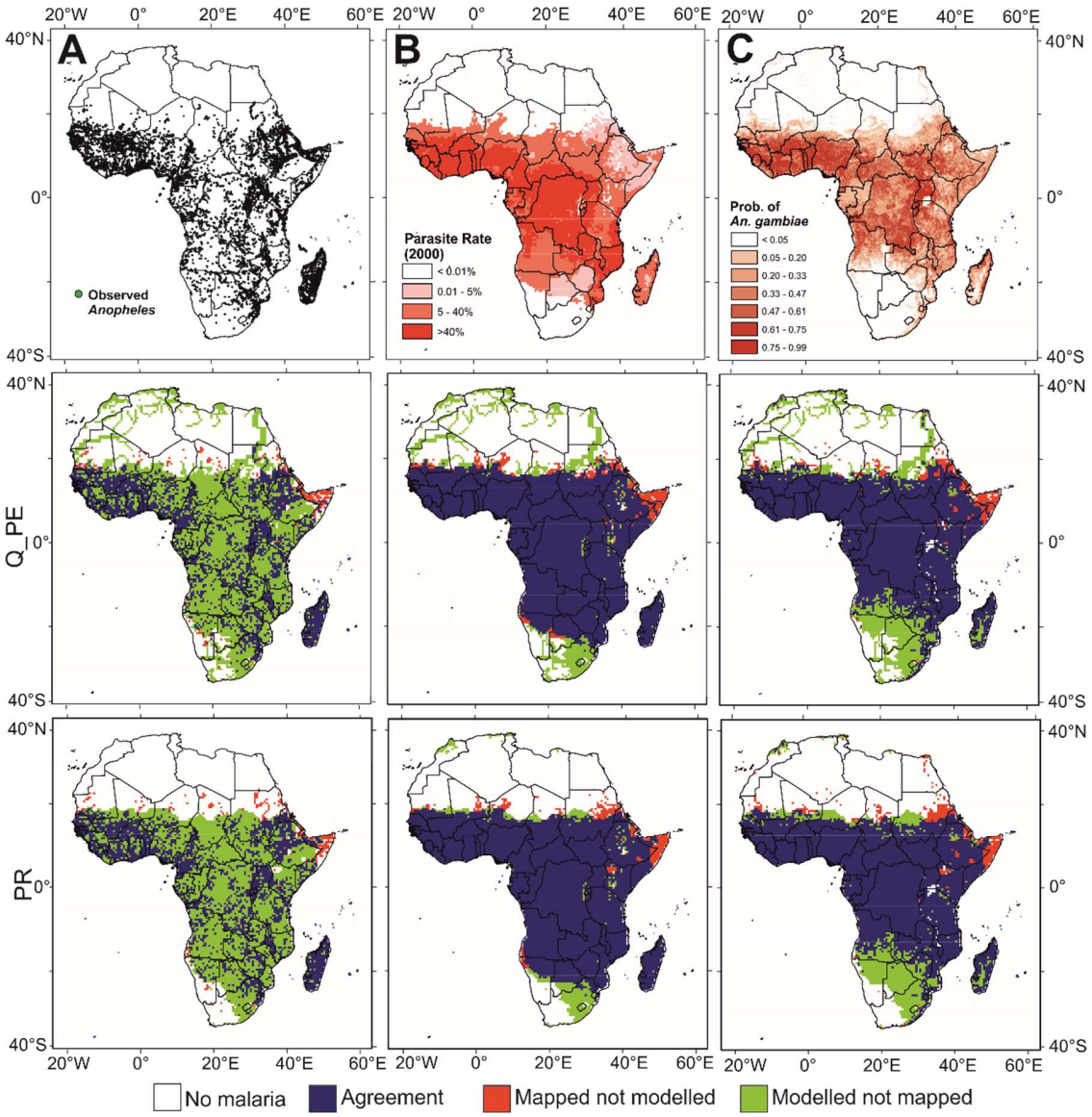

Fig. S9.
Validation of weighted malaria suitability estimates (for discharge with potential evaporation and precipitation-based estimates) against more recent data sources for 'All malaria' (>1 month suitability) transmission suitability calculated over the time period 1986-2005. (A) Kyalo et al. (*36*) anopheles inventory of sub-Saharan Africa (1898-2016) displaying all observations of anophelines. (B) Malaria Atlas Project modelled estimates of parasite rate from Bhatt et al. (*37*) for 2000. (C) Wiebe et al. (*38*) estimate of the mean modelled relative probability of occurrence of *Anopheles gambiae*.

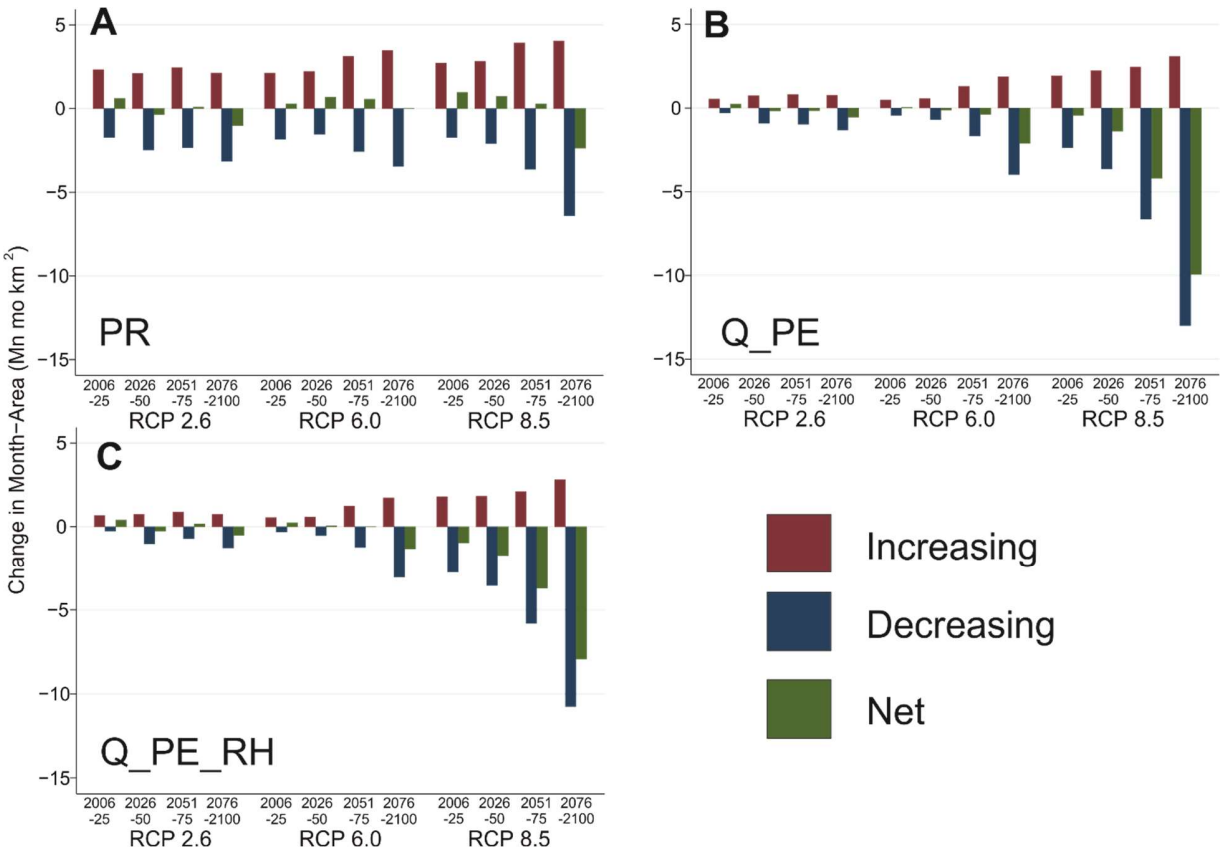

Fig. S10.

Projected changes from 1985-2005 in malaria suitability 'month-areas' suitable (in millions mo km^2) in future projections where the areas are multiplied by the number of months change in malaria climatic suitability to provide a clearer indication of the magnitude of changes) for each time period, RCP and hydrological representation.

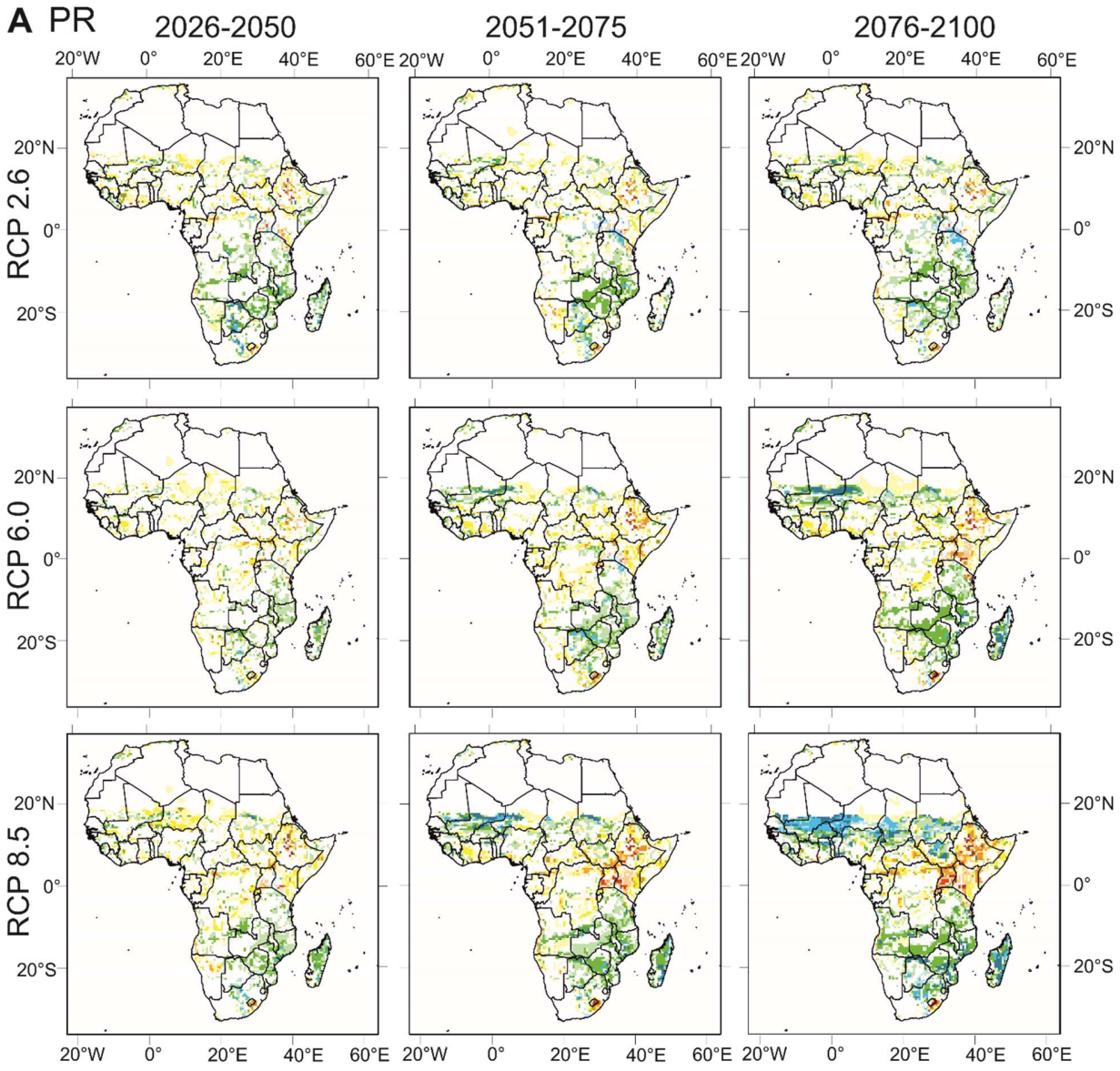
A PR
2026-2050
2051-2075
2076-2100
RCP 2.6
RCP 6.0
RCP 8.5
20°W
0°
20°E
40°E
60°E
20°N
0°
20°S

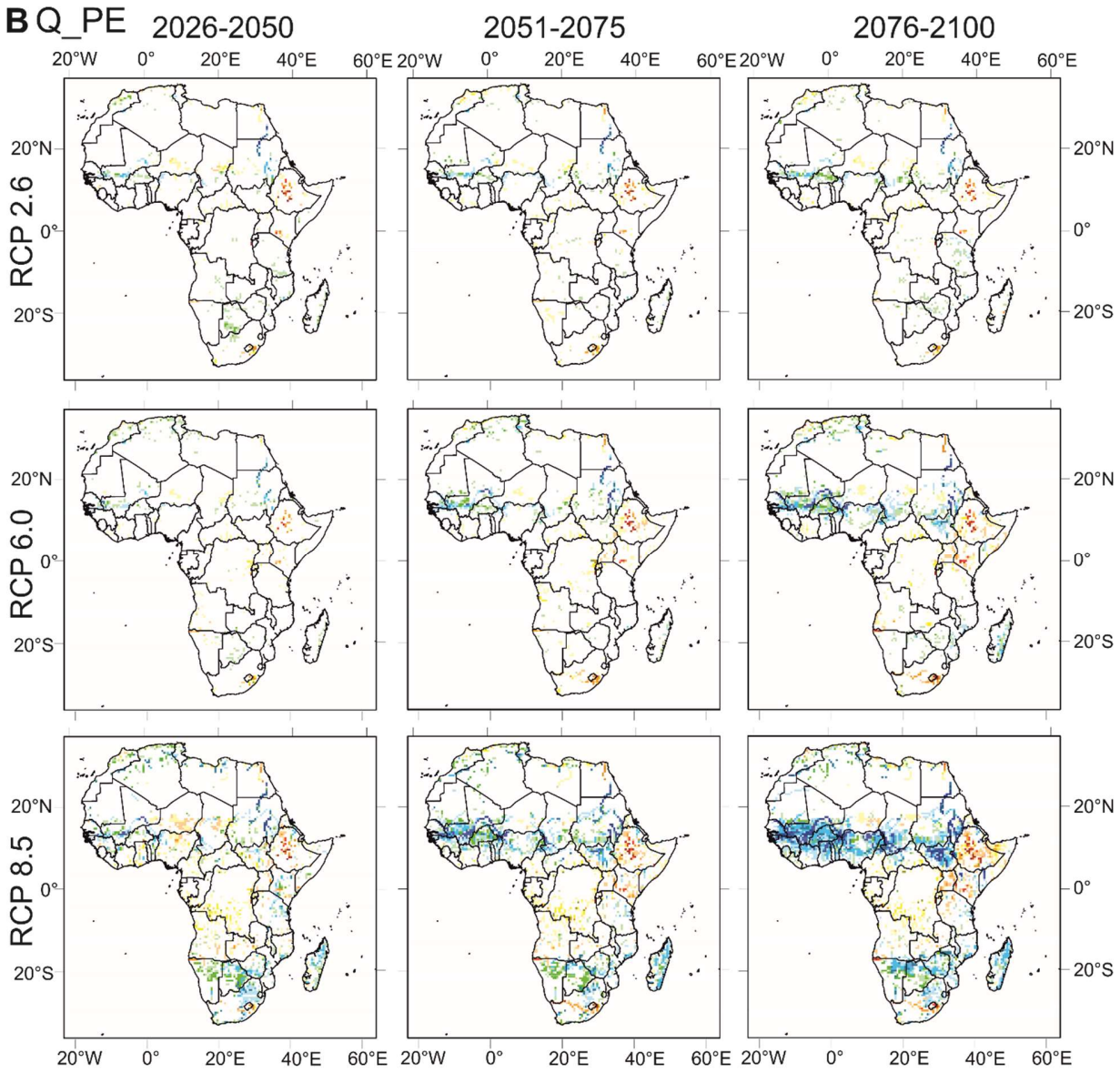
B Q_PE
2026-2050
2051-2075
2076-2100
RCP 2.6
RCP 6.0
RCP 8.5
20°W
0°
20°E
40°E
60°E
20°N
0°
20°S

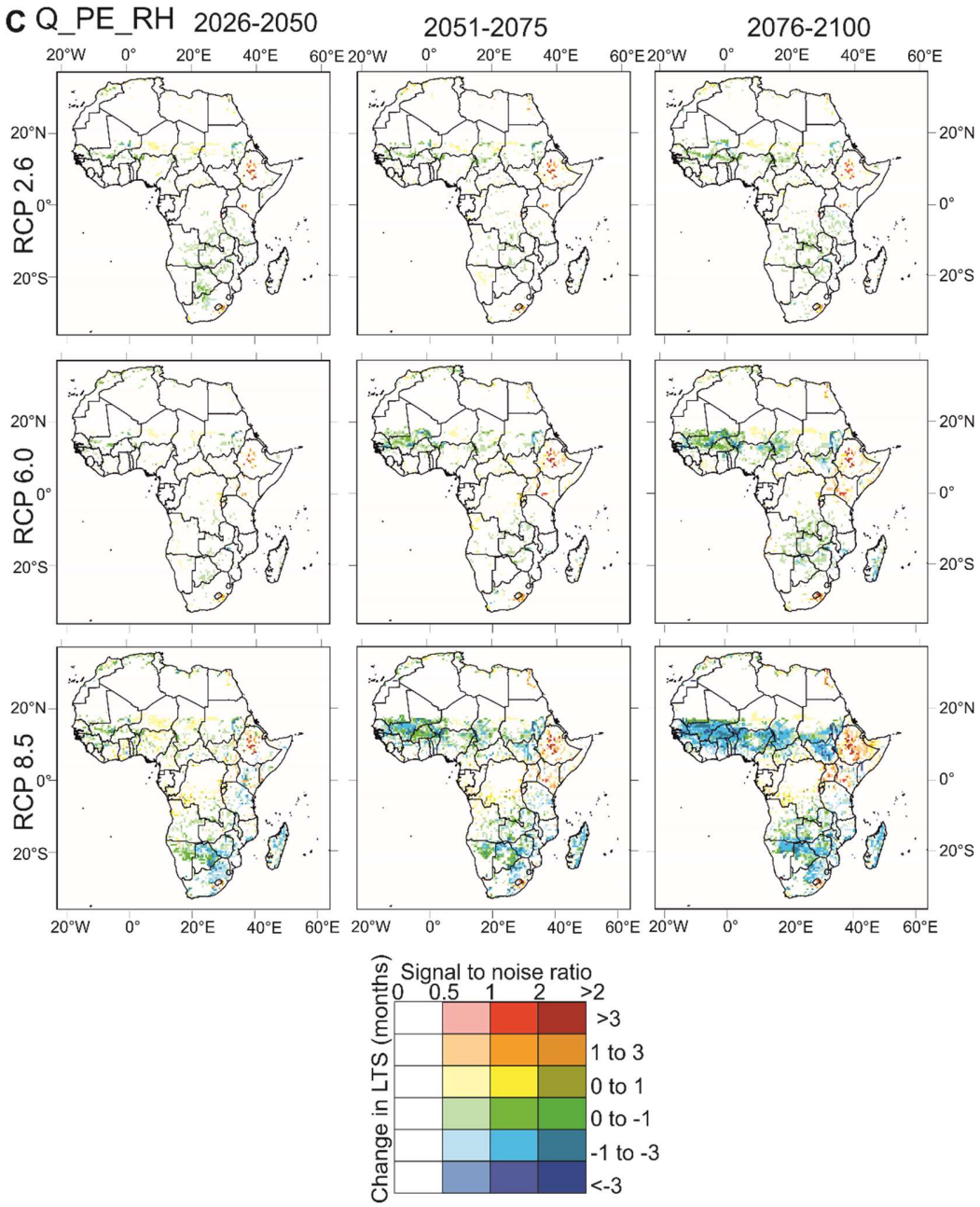

Fig. S11.

Changes in duration of malaria transmission climatic suitability between the period 1985-2005 and each future period for each RCP and hydrological representation. Different saturations indicate the signal-to-noise ratio across the model ensemble, with the noise defined as the standard deviation of estimates across the projections, as per Fig. 3.

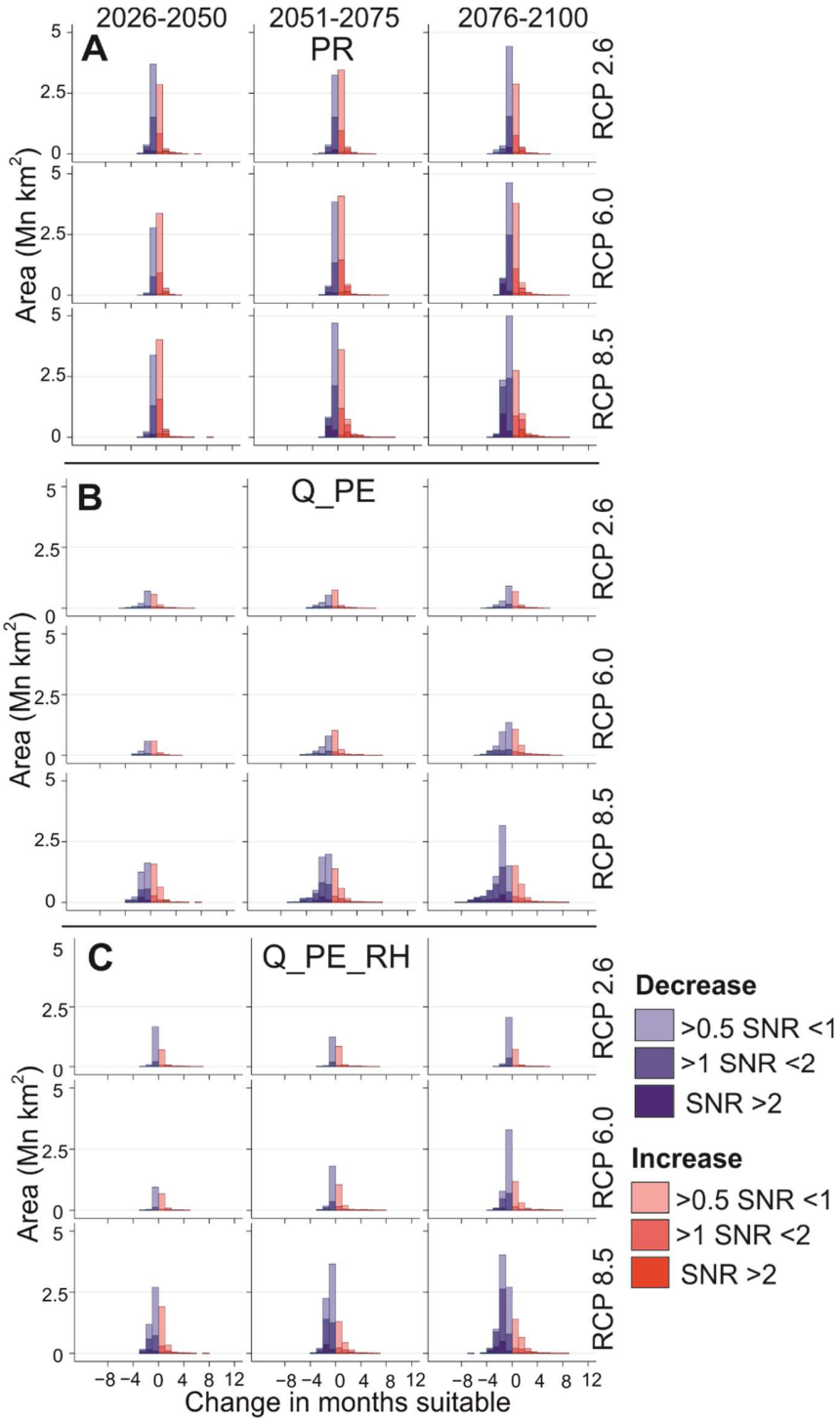

Fig. S12.

Areas with changing malaria transmission suitability. Stacked histograms showing changes in number of months climatically suitable between the period 1985-2005 and all future time periods for each RCPs and hydrological representation, split into categories of signal-to-noise ratio as per Fig. 3.

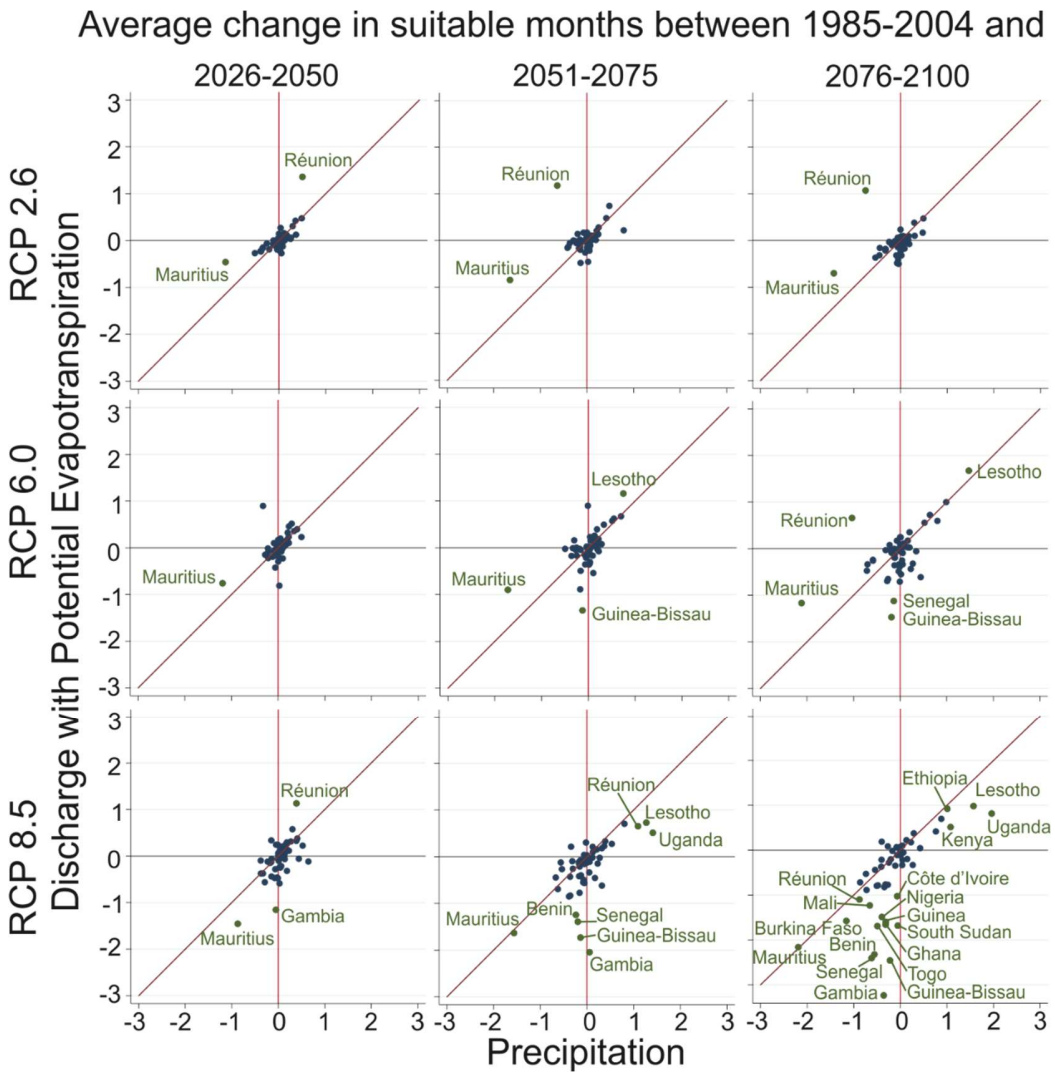

Fig. S13.

By-country comparison of average changes in malaria transmission suitability season length between the period 1985-2005 and each future period. Discharge and potential evapotranspiration and precipitation-based estimates are plotted on separate axes and the 1:1 line shown in red. Countries with an estimated average change of >1 month are named in each plot.

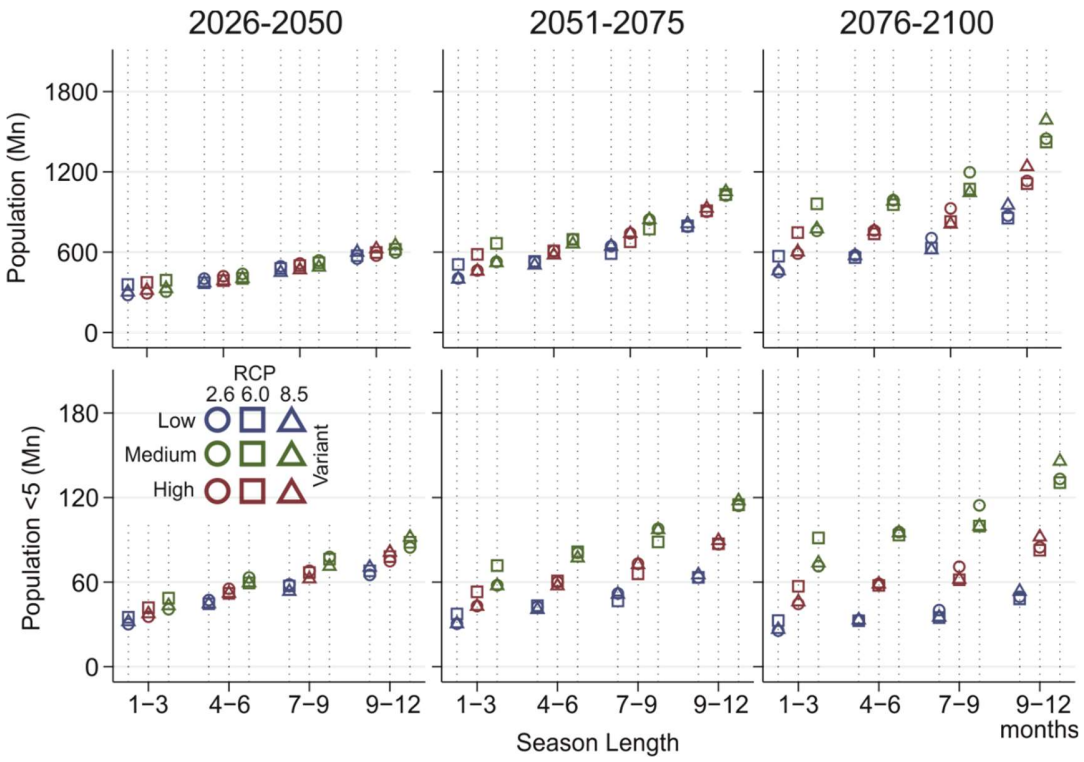

Fig. S14.

Comparison of UN population variants. The effect of UN population variant (High, Medium or Low) on future population predictions of malaria suitability in Africa for the discharge with potential evapotranspiration (Q_PE) hydrological representation. Results from each RCP are displayed separately.

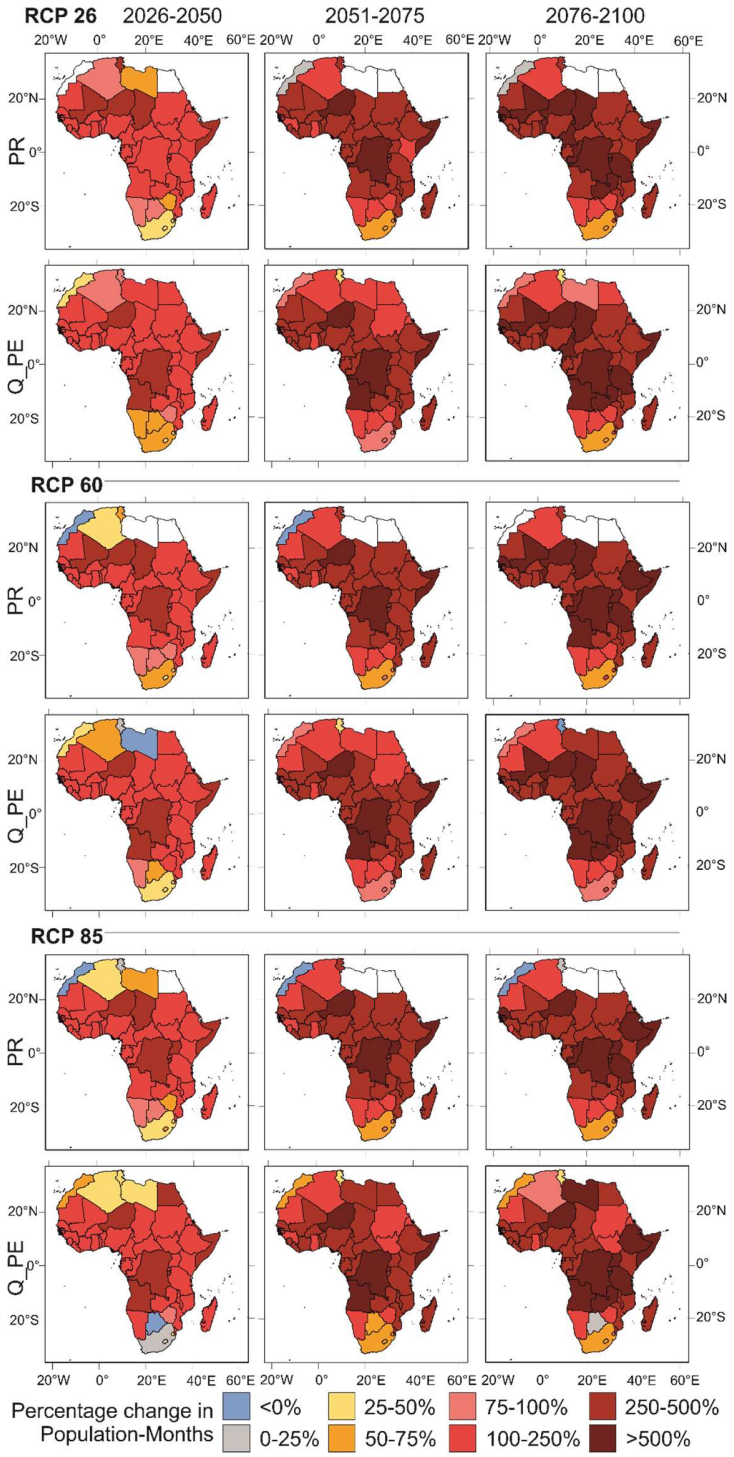

Fig. S15.

Predicted percentage changes in population-months (i.e., population exposed multiplied by the number of additional months of exposure) since 1986-2005 by country and for each RCP. White shading indicates no estimated malaria suitability.

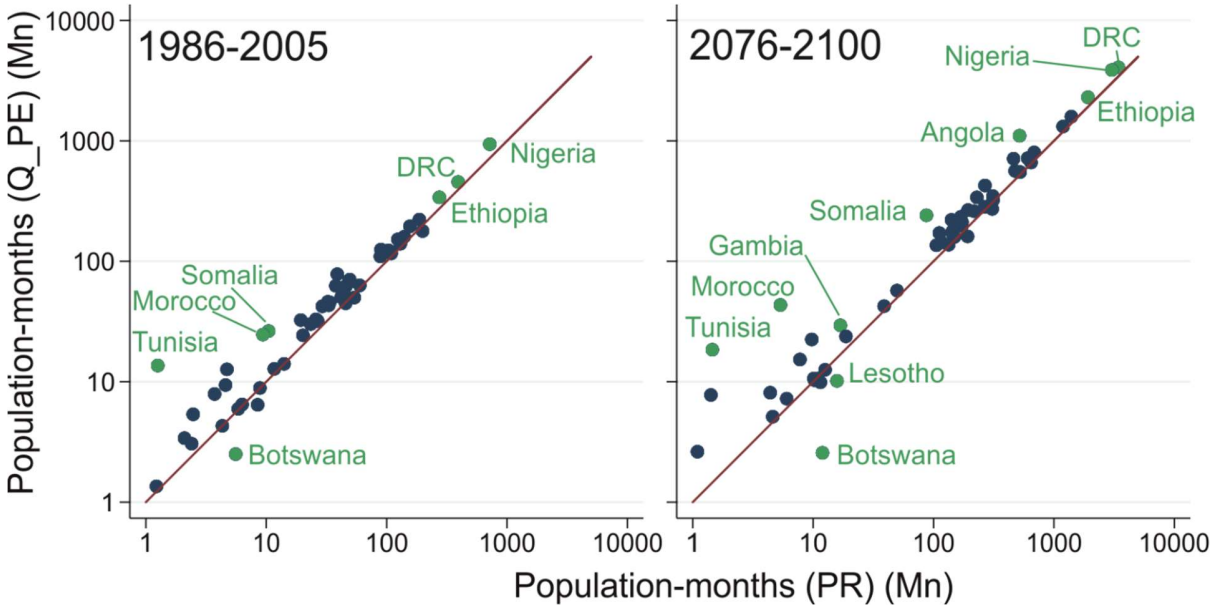

Fig. S16.

Country-by-country comparison of population-months. Comparison of population-month estimates (i.e., population exposed multiplied by the number of additional months of exposure) from the Q_PE and PR hydrological representations is presented for both the historical period 1986-2005 (using population estimates) and 2076-2100 (using RCP 8.5 and the Medium UN population estimates). The 1:1 line is shown in red. Individual countries are highlighted when a large difference in predictions is observed or for countries with high overall values.

Table S1. Areas of different model agreement levels for model ensembles for each hydrological representation (areas stated in Mn km^2) and four malaria season length classifications: 'All' (LTS >1 month), 'Stable' (LTS > 3 months), 'Seasonal' (LTS > 6 months) and 'Endemic' (LTS > 9 months).

Malaria level	Hydrology	Total Models	No Models Predict	Minority Agree	Majority Agree	All Models Agree
All	PR	4	10.13	0.63	0.79	18.26
	Q	27	9.14	7.45	7.47	5.75
	PE	23	10.11	2.43	1.97	15.30
	Q_PE	23	7.28	4.23	2.48	15.82
	Q_RH	27	10.58	6.19	7.35	5.68
	Q_PE_RH	23	8.57	3.19	2.33	15.72
Stable	PR	4	14.67	0.63	0.76	13.74
	Q	27	11.92	7.25	6.16	4.48
	PE	23	14.96	2.23	1.86	10.75
	Q_PE	23	10.37	4.95	2.58	11.91
	Q_RH	27	14.47	5.28	5.87	4.19
	Q_PE_RH	23	12.62	3.05	2.39	11.74
Seasonal	PR	4	21.94	0.61	0.59	6.67
	Q	27	14.41	8.09	4.74	2.57
	PE	23	21.29	2.26	1.57	4.68
	Q_PE	23	13.38	5.74	3.53	7.16
	Q_RH	27	17.67	5.80	4.20	2.14
	Q_PE_RH	23	16.64	3.59	3.06	6.51
Endemic	PR	4	27.57	0.39	0.24	1.61
	Q	27	17.04	7.69	3.92	1.17
	PE	23	26.79	1.37	0.74	0.91
	Q_PE	23	16.91	6.20	3.49	3.21
	Q_RH	27	21.02	4.85	2.94	1.00
	Q_PE_RH	23	20.81	3.59	2.52	2.88

Table S2. Ensemble Score validation metric (Equ. 4) for each model for 'All malaria' (>1 month suitability) transmission suitability based on the pre-intervention (~1900) map of Lysenko and Semashko (*32*). The final row shows the ensemble score for the final weighted ensembles.

GCM	Hydrological Model	PR	Q	PE	Q_PE	Q_RH	Q_PE_RH
GFDL	-	0.816	-	-	-	-	-
	CLM45	-	0.533	-	-	0.526	-
	H08	-	0.529	0.730	0.753	0.522	0.746
	LPJ	-	0.676	0.732	0.782	0.661	0.774
	MPI_HM	-	0.270	0.790	0.810	0.260	0.802
	ORCHIDEE	-	0.593	0.708	0.750	0.588	0.748
	PCR_GLOWB	-	0.509	0.806	0.817	0.506	0.819
	WATERGAP2	-	0.507	0.747	0.775	0.500	0.773
HadGEM	-	0.808	-	-	-	-	-
	CLM45	-	0.584	-	-	0.575	-
	H08	-	0.572	0.745	0.766	0.565	0.760
	LPJ	-	0.703	0.739	0.784	0.681	0.769
	ORCHIDEE	-	0.635	0.717	0.762	0.628	0.759
	PCR_GLOWB	-	0.541	0.792	0.809	0.537	0.809
	WATERGAP2	-	0.562	0.746	0.784	0.554	0.778
IPSL	-	0.784	-	-	-	-	-
	CLM45	-	0.530	-	-	0.525	-
	H08	-	0.522	0.717	0.738	0.517	0.733
	LPJ	-	0.653	0.703	0.760	0.635	0.745
	MPI_HM	-	0.265	0.767	0.784	0.255	0.776
	ORCHIDEE	-	0.592	0.686	0.734	0.582	0.730
	PCR_GLOWB	-	0.506	0.784	0.799	0.501	0.798
	WATERGAP2	-	0.495	0.721	0.759	0.485	0.750
MIROC5	-	0.816	-	-	-	-	-
	CLM45	-	0.547	-	-	0.540	-
	H08	-	0.538	0.728	0.749	0.532	0.744
	LPJ	-	0.675	0.737	0.787	0.658	0.776
	MPI_HM	-	0.279	0.790	0.806	0.270	0.800
	ORCHIDEE	-	0.613	0.725	0.765	0.608	0.765
	PCR_GLOWB	-	0.538	0.809	0.821	0.535	0.822
	WATERGAP2	-	0.530	0.752	0.780	0.525	0.778
WEIGHTED ENSEMBLE		0.816	0.723	0.782	0.817	0.698	0.808

Table S3. Ensemble Score validation metric (Equ. 4) for each model for 'Mesoendemic' (>3 months) transmission suitability based on the pre-intervention (~1900) map of Lysenko and Semashko (*32*).

GCM	Hydrological Model	PR	Q	PE	Q_PE	Q_RH	Q_PE_RH
GFDL	-	0.777	-	-	-	-	-
	CLM45	-	0.596	-	-	0.598	-
	H08	-	0.560	0.730	0.751	0.562	0.757
	LPJ	-	0.653	0.700	0.762	0.648	0.770
	MPI_HM	-	0.316	0.769	0.774	0.309	0.779
	ORCHIDEE	-	0.639	0.705	0.756	0.651	0.773
	PCR_GLOWB	-	0.495	0.762	0.724	0.512	0.765
	WATERGAP2	-	0.489	0.724	0.744	0.491	0.759
HadGEM	-	0.751	-	-	-	-	-
	CLM45	-	0.631	-	-	0.629	-
	H08	-	0.569	0.732	0.756	0.569	0.761
	LPJ	-	0.670	0.707	0.764	0.666	0.766
	ORCHIDEE	-	0.685	0.698	0.756	0.692	0.776
	PCR_GLOWB	-	0.531	0.738	0.706	0.545	0.736
	WATERGAP2	-	0.525	0.708	0.740	0.522	0.747
IPSL	-	0.765	-	-	-	-	-
	CLM45	-	0.605	-	-	0.605	-
	H08	-	0.567	0.724	0.751	0.570	0.756
	LPJ	-	0.672	0.689	0.766	0.666	0.771
	MPI_HM	-	0.321	0.756	0.766	0.319	0.770
	ORCHIDEE	-	0.655	0.696	0.750	0.665	0.763
	PCR_GLOWB	-	0.517	0.750	0.735	0.532	0.765
	WATERGAP2	-	0.504	0.705	0.742	0.506	0.752
MIROC5	-	0.765	-	-	-	-	-
	CLM45	-	0.614	-	-	0.614	-
	H08	-	0.565	0.719	0.745	0.569	0.751
	LPJ	-	0.667	0.696	0.766	0.663	0.772
	MPI_HM	-	0.327	0.756	0.762	0.323	0.766
	ORCHIDEE	-	0.676	0.720	0.766	0.692	0.790
	PCR_GLOWB	-	0.535	0.747	0.722	0.554	0.762
	WATERGAP2	-	0.529	0.711	0.745	0.530	0.753

Table S4. Optimum number of model agreements used to award maximum weight to the best performing models up to that limit (following (*73*)) for each hydrological representation and a range metrics.

Hydrological Representation	Optimum agreement levels					
	Ensemble Score		F^2		Bias	
	All	Mesoendemic	All	Mesoendemic	All	Mesoendemic
PR	1	1	1	1	1	2
Q	1	5	1	5	1	5
PE	1	3	1	3	1	2
Q_PE	3	9	3	9	3	9
Q_RH	1	2	1	1	1	3
Q_PE_RH	2	6	2	5	1	7

Table S5. Weights applied to model ensemble for each hydrological representation.

GCM	Hydrological Model	Q	PE	Q_RH	Q_PE	Q_PE_RH
GFDL PR 0.4244	CLM45	0.0393		0.0394		
	H08	0.0364	0.0409	0.0365	0.0299	0.0234
	LPJ	0.0533	0.0230	0.0522	0.0550	0.0465
	MPI_HM	0.0004	0.0863	0.0003	0.0740	0.0752
	ORCHIDEE	0.0466	0.0177	0.0475	0.0308	0.0477
	PCR_GLOWB	0.0301	0.0921	0.0318	0.0514	0.0677
	WATERGAP2	0.0295	0.0436	0.0299	0.0376	0.0381
HadGEM PR 0.1337	CLM45	0.0454		0.0450		
	H08	0.0399	0.0474	0.0399	0.0387	0.0330
	LPJ	0.0576	0.0301	0.0549	0.0559	0.0417
	ORCHIDEE	0.0530	0.0169	0.0532	0.0451	0.0532
	PCR_GLOWB	0.0350	0.0680	0.0363	0.0371	0.0408
	WATERGAP2	0.0360	0.0330	0.0358	0.0405	0.0324
IPSL PR 0.1283	CLM45	0.0399		0.0398		
	H08	0.0364	0.0325	0.0368	0.0226	0.0155
	LPJ	0.0542	0.0062	0.0518	0.0438	0.0458
	MPI_HM	0.0004	0.0781	0.0007	0.0557	0.0479
	ORCHIDEE	0.0478	0.0047	0.0481	0.0201	0.0186
	PCR_GLOWB	0.0316	0.0725	0.0329	0.0455	0.0554
	WATERGAP2	0.0299	0.0224	0.0299	0.0292	0.0220
MIROC5 PR 0.3136	CLM45	0.0417		0.0415		
	H08	0.0374	0.0331	0.0377	0.0254	0.0177
	LPJ	0.0558	0.0229	0.0531	0.0572	0.0616
	MPI_HM	0.0018	0.0783	0.0020	0.0665	0.0571
	ORCHIDEE	0.0515	0.0333	0.0518	0.0466	0.0561
	PCR_GLOWB	0.0351	0.0797	0.0368	0.0504	0.0654
	WATERGAP2	0.0341	0.0370	0.0344	0.0410	0.0371

Table S6. Validation of weighted malaria suitability estimates against more recent data sources for 'All malaria' (>1 month suitability) transmission suitability calculated over the time period 1986-2005.

Hydrological Representation	Percentage of positive occurrences correctly identified by malaria suitability model		
	Anopheles inventory of sub-Saharan Africa (1898-2016) from Kyalo et al. (*29*)	Malaria Atlas Project modelled estimates of parasite rate for 2000 from Bhatt et al. (*30*)	estimate of the mean modelled relative probability of occurrence of *Anopheles gambiae* by Wiebe et al. (*31*)
PR	93.1	95.3	94.1
Q	84.7	85.2	87.5
PE	89.9	91.9	91.4
Q_PE	93.3	94.6	94.6
Q_RH	82.5	83.1	85.6
Q_PE_RH	92.1	94.2	93.8

Table S7. Areas estimated to be hydro-climatically suitable for malaria transmission by the weighted ensembles of each hydrological representation for each RCP and time period. Areas suitable for > 1 month ('All') and > 3 months (i.e., stable areas) are calculated.

	Total Area (Mn km^2)			Stable Area (Mn km^2)		
	Q_PE	PR	Q_PE_RH	Q_PE	PR	Q_PE_RH
1875-1900	19.825	18.907	18.457	14.646	13.863	13.968
1986-2005	19.315	18.776	18.121	14.588	14.113	13.936
RCP 2.6						
2006-2025	19.814	19.011	18.396	14.675	14.252	14.031
2026-2050	19.486	18.762	18.127	14.521	13.892	13.828
2051-2075	19.579	18.953	18.338	14.544	14.057	13.869
2076-2100	19.466	18.733	18.176	14.298	13.814	13.626
RCP 6.0						
2006-2025	19.544	18.979	18.367	14.570	14.182	13.901
2026-2050	19.312	18.773	18.089	14.515	14.147	13.855
2051-2075	19.307	18.724	18.156	14.530	13.901	13.872
2076-2100	19.205	18.362	17.976	14.281	13.773	13.620
RCP 8.5						
2006-2025	19.170	19.034	17.857	14.408	13.979	13.773
2026-2050	19.109	18.843	17.692	14.353	14.139	13.579
2051-2075	19.049	18.486	17.547	14.055	13.521	13.315
2076-2100	18.892	17.895	17.240	13.455	13.037	12.785

Table S8. Changes in total (suitable for > 1 month) and stable areas (suitable for > 3 months) between the historical period (1985-2005) and each time period. Results for each weighted ensemble are presented.

	Total Area (Mn km^2)			Stable Area (Mn km^2)		
	Q_PE	PR	Q_PE_RH	Q_PE	PR	Q_PE_RH
RCP 2.6						
2006-2025	0.499	0.235	0.275	0.087	0.139	0.096
2026-2050	0.171	-0.014	0.006	-0.067	-0.220	-0.107
2051-2075	0.264	0.177	0.217	-0.043	-0.055	-0.067
2076-2100	0.151	-0.043	0.055	-0.290	-0.299	-0.310
RCP 6.0						
2006-2025	0.229	0.203	0.246	-0.017	0.070	-0.035
2026-2050	-0.003	-0.003	-0.032	-0.072	0.035	-0.081
2051-2075	-0.009	-0.052	0.035	-0.058	-0.212	-0.064
2076-2100	-0.110	-0.414	-0.145	-0.307	-0.339	-0.316
RCP 8.5						
2006-2025	-0.145	0.258	-0.264	-0.180	-0.133	-0.162
2026-2050	-0.206	0.067	-0.429	-0.235	0.026	-0.357
2051-2075	-0.267	-0.290	-0.574	-0.533	-0.591	-0.620
2076-2100	-0.423	-0.881	-0.881	-1.133	-1.075	-1.151

Table S9. Areas (in Mn km^2) experiencing an increase and decrease in malaria suitability in future ensemble projections since the historical period (1985-2005). Note that the net value includes areas with an average change of <1 month and only where the signal to noise ratio >0.5.

	Q_PE			PR			Q_PE_RH		
	Increasing	Decreasing	Net	Increasing	Decreasing	Net	Increasing	Decreasing	Net
RCP 2.6									
2006-2025	0.710	0.328	0.383	3.658	2.907	0.751	0.971	0.493	0.478
2026-2050	0.771	0.991	-0.220	3.188	4.087	-0.899	0.890	1.791	-0.901
2051-2075	0.942	0.901	0.041	3.840	3.669	0.171	1.070	1.307	-0.238
2076-2100	0.878	1.356	-0.478	3.246	4.936	-1.690	0.910	2.220	-1.310
RCP 6.0									
2006-2025	0.661	0.530	0.130	3.551	2.954	0.597	0.803	0.580	0.223
2026-2050	0.733	0.806	-0.072	3.698	2.875	0.823	0.809	0.977	-0.168
2051-2075	1.368	1.403	-0.035	4.649	4.255	0.394	1.359	2.017	-0.658
2076-2100	1.672	2.939	-1.267	4.539	5.380	-0.841	1.664	4.168	-2.504
RCP 8.5									
2006-2025	2.206	2.539	-0.333	4.177	2.890	1.287	2.510	3.307	-0.797
2026-2050	2.380	3.206	-0.826	4.452	3.646	0.806	2.345	4.052	-1.707
2051-2075	2.238	4.748	-2.510	4.635	5.542	-0.907	1.980	6.139	-4.159
2076-2100	2.603	6.823	-4.220	4.058	7.516	-3.458	2.380	7.965	-5.585

Table S10. Increase and decrease in malaria suitability 'month-areas' (in millions mo km^2) between future projections and the historical period (1985-2005). Areas used to calculate totals in Table S9 are multiplied by the number of months change in malaria climatic suitability to provide a clearer indication of the magnitude of changes.

	Q_PE			PR			Q_PE_RH		
	Increasing	Decreasing	Net	Increasing	Decreasing	Net	Increasing	Decreasing	Net
RCP 2.6									
2006-2025	0.532	-0.297	0.235	2.333	-1.726	0.607	0.668	-0.264	0.404
2026-2050	0.742	-0.913	-0.171	2.101	-2.472	-0.371	0.746	-1.014	-0.268
2051-2075	0.816	-0.975	-0.159	2.439	-2.339	0.100	0.874	-0.709	0.165
2076-2100	0.770	-1.325	-0.555	2.127	-3.155	-1.027	0.748	-1.270	-0.522
RCP 6.0									
2006-2025	0.481	-0.442	0.039	2.123	-1.839	0.284	0.555	-0.310	0.245
2026-2050	0.572	-0.693	-0.120	2.226	-1.548	0.678	0.587	-0.535	0.052
2051-2075	1.296	-1.672	-0.377	3.130	-2.574	0.557	1.239	-1.249	-0.010
2076-2100	1.874	-3.974	-2.100	3.464	-3.455	0.009	1.725	-3.061	-1.336
RCP 8.5									
2006-2025	1.926	-2.374	-0.448	2.709	-1.738	0.971	1.794	-2.761	-0.967
2026-2050	2.242	-3.623	-1.381	2.829	-2.104	0.725	1.827	-3.553	-1.726
2051-2075	2.458	-6.646	-4.188	3.914	-3.632	0.283	2.094	-5.817	-3.723
2076-2100	3.078	-13.005	-9.927	4.040	-6.413	-2.372	2.816	-10.756	-7.940

Table S11. Total populations (Mn) and children under 5 years old within areas of climatic suitability for malaria transmission in Africa (>1 month) and climatic suitability for stable malaria transmission (>3 months). Population figures are calculated from the mid-point of each time period using the UN Medium Variant figures, except 2006-2025 which use Worldpop gridded estimates.

	LTS >1 month			LTS >3 months		
	Q_PE	PR	Q_PE_RH	Q_PE	PR	Q_PE_RH
Total Population (Mn)						
RCP 2.6						
2006-2025	1060.8	990.4	1034.4	866.4	826.9	845.5
2026-2050	1803.0	1716.2	1765.8	1510.5	1414.3	1466.7
2051-2075	2714.8	2610.7	2663.0	2251.7	2118.0	2183.8
2076-2100	3410.6	3292.9	3345.9	2821.1	2632.1	2705.0
RCP 6.0						
2006-2025	1059.6	994.2	1031.8	850.0	807.7	821.5
2026-2050	1794.9	1710.0	1747.9	1479.8	1401.8	1447.5
2051-2075	2704.9	2597.6	2658.7	2247.0	2122.1	2177.4
2076-2100	3407.6	3276.6	3337.3	2805.3	2678.1	2698.5
RCP 8.5						
2006-2025	1083.0	997.9	1039.5	850.7	814.2	832.5
2026-2050	1860.1	1717.5	1791.3	1485.4	1417.7	1434.5
2051-2075	2780.0	2601.2	2717.8	2196.2	2071.0	2119.3
2076-2100	3424.6	3229.0	3325.7	2678.4	2515.3	2548.1
Under 5s (Mn)						
RCP 2.6						
2006-2025	172.0	163.6	168.2	143.9	137.7	140.2
2026-2050	233.7	226.2	229.6	198.2	186.2	192.3
2051-2075	262.8	255.9	258.4	219.9	207.3	212.5
2076-2100	258.9	252.2	254.4	214.4	200.9	204.9
RCP 6.0						
2006-2025	171.9	164.0	167.8	140.7	134.5	135.7
2026-2050	233.0	225.6	228.0	195.5	185.4	190.4
2051-2075	262.1	255.0	258.1	219.3	206.9	212.1
2076-2100	258.6	251.0	253.4	212.6	202.7	203.7
RCP 8.5						
2006-2025	175.0	164.5	169.3	142.2	135.9	138.9
2026-2050	238.7	226.5	232.0	196.9	187.1	189.7
2051-2075	267.1	255.0	261.7	214.0	201.0	205.6
2076-2100	259.0	246.9	251.7	202.0	189.0	191.5